


Causes and implications of Mid- to Late Holocene relative sea-level change in the Gulf of Kachchh, western India

Shubhra Sharma^{a*}, Gaurav Chauhan^b, Anil Dutt Shukla^a, Romi Nambiar^a, Ravi Bhushan^a, Bhawanisingh G. Desai^c, Shilpa Pandey^d, Madhavi Dabhi^b, Subhash Bhandari^b, Suraj Bhosale^b, Abhishek Lakhote^b, Navin Juyal^a

^aPhysical Research Laboratory, Ahmedabad-380009, India

^bDepartment of Earth and Environmental Science, The K.S.K.V. Kachchh University, Bhuj-370001, India

^cPandit Deendayal Petroleum University, Raisan Village, Gandhinagar-382009, India

^dBirbal Sahni Institute of Palaeoscience, Lucknow-226007, India

*Corresponding author at: Department of Geography, Banaras Hindu University, Varanasi, India-221005. E-mail address: shubshubhra@gmail.com; shubhra@bhu.ac.in (S. Sharma).

(RECEIVED October 23, 2019; ACCEPTED August 19, 2020)

Abstract

The relict intertidal deposits from the Kharod River Estuary, Gulf of Kachchh, and the distal end of Kori Creek are used to infer the Mid- to Late Holocene relative sea-level (RSL) change in western India. Employing sedimentology, geochemistry, palynology, ichnology, and optical and radiocarbon dating, the study suggests the dominance of fluvial activity between 16.5 ± 1.6 and 9.9 ± 0.7 ka. After ~ 7 ka (7.3 ± 0.4 , 6.8 ± 0.5 ka), the sea level showed a positive tendency until 4.7 ± 0.2 ka. The tectonically corrected Mid-Holocene RSL change is estimated as 1.45 ± 0.33 m between ~ 7 and ~ 5 ka. The study suggests that the Mid-Holocene RSL high was due to the meltwater contribution from the Himalayan cryosphere, with subordinate contribution from glacio-isostatic adjustment and crustal subsidence. The Late Holocene tectonically corrected RSL change at ~ 1 ka (1.1 ± 0.1 ka and 1045 ± 175 cal yr BP) is estimated as 0.53 ± 0.43 m. This is ascribed to monsoon wind-driven tidal ingression that might have affected the tidal amplitude positively. The study suggests that the Mid-Holocene RSL change did not play a deterministic role in the abandonment of the Harappan coastal settlements.

Keywords: Relative sea-level change; Intertidal deposits; Gulf of Kachchh; Mid- to Late Holocene; Indian Summer Monsoon

INTRODUCTION

It has been suggested that the Holocene sea level was modulated by a combination of factors that perturbed the land-sea configuration (Lambeck et al., 2014; Vacchi et al., 2014; Engelhart et al., 2015). These include tectonic instability, coastal configuration changes, proximity of the sites to meltwater discharge, sediment flux, and most importantly the post-last glacial maximum (LGM) glacio-isostatic adjustment (GIA) in the higher latitudes (Newman et al., 1989; Shennan and Horton, 2002; Ferrier et al., 2015). Therefore, a generalized global time/depth Holocene sea-level curve would be misleading (Pirazzoli, 1991). To ascertain the eustatic component (glacial melt and hence the climate) for Holocene relative sea-level (RSL) change, it is suggested

that the focus should be on tectonically stable and far-field locations from the LGM ice margins (Clark et al., 1978).

In the far-field locations (away from ice sheets), the GIA depends significantly on equatorial ocean siphoning and hydro-isostasy (continental levering) (Clark et al., 1978; Newman et al., 1989; Mitrovica and Milne, 2002; Shennan and Horton, 2002; Ferrier et al., 2015). Equatorial ocean siphoning redistributes ocean water from the equator to higher latitudes because of subsiding peripheral fore-bulges and sub-lithospheric mantle flow (Mitrovica and Peltier, 1991; Peltier, 1999). Continental levering refers to hydro-isostatic subsidence of the oceanic crust and uplift of coastlines (Mitrovica and Milne, 2002; Mann et al., 2019). Researchers have argued that these processes were important, particularly for the Late Holocene RSL fall in the low latitudes (Mitrovica and Milne, 2002), including the Indian Ocean (Woodroffe et al., 1990; Kench et al., 2009). Therefore, to ascertain the eustatic component, the non-eustatic components need to be accounted for (Mitrovica and Peltier, 1991).

Along the Indian coast, limited studies suggest significant changes in the magnitude of the Holocene sea level

¹Current Address: Department of Geography, Banaras Hindu University, Varanasi, India-221005

Cite this article: Sharma, S. et al 2021. Causes and implications of Mid- to Late Holocene relative sea-level change in the Gulf of Kachchh, western India. *Quaternary Research* 100, 98–121. <https://doi.org/10.1017/qua.2020.86>

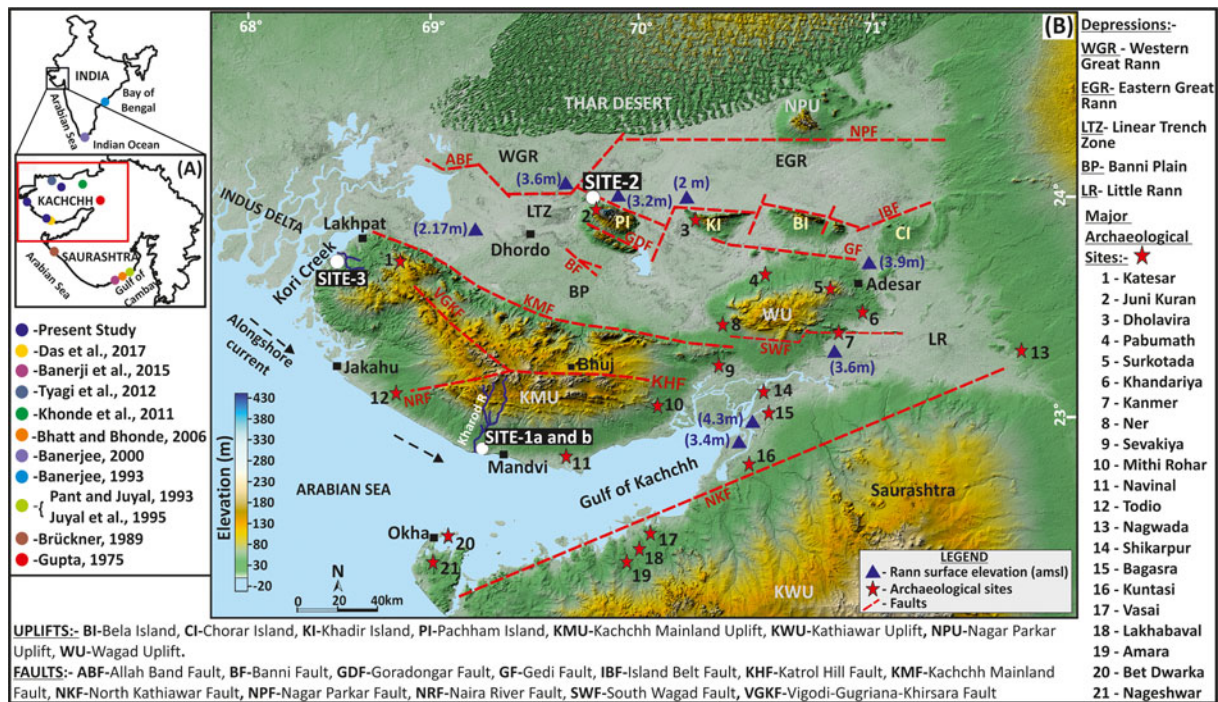


Figure 1. In the inset map of India and (A) Gulf of Kachchh region, the colored dots mark the locations of various studies. The red rectangle marks the location of the enlarged map. (B) Digital Elevation Map of Kachchh peninsula showing major and minor thrusts (modified after Biswas, 2016). Sites investigated in the present study are marked in white circles: the Kharod Estuary (Site-1a), the river section (Site-1b), the India Bridge section (Site-2), and the Nani Cher Estuary section (Site-3). (For interpretation of the references to color in this figure legend, the reader is referred to the web version of this article.)

(Banerjee, 1993, 2000; Pant and Juyal, 1993; Juyal et al., 1995; Kunte and Wagle, 2005; Bhatt and Bhonde, 2006; Banerji et al., 2015) (Fig. 1A). Banerjee (2000) estimated Holocene sea level from the passive margin boundary (tectonically stable) on the eastern Indian coast. The study suggests an ~3 m high stand above low tide level at ~7 ka, and an ~1 m high stand between 5.2 and 4.2 ka. From the tectonically active western coast of India (Saurashtra peninsula), the chronology of the raised oyster beds indicates that Holocene sea level fluctuated between 2 and 3 m above mean sea level (amsl) from 8.6 to 2.5 ka (Pant and Juyal, 1993; Juyal et al., 1995). More recently, Banerji et al. (2015), after accounting for the tectonic component, suggested that the Mid-Holocene sea level in the Saurashtra Peninsula was ~1 m higher than the present. A similar observation was made by Brückner (1989), suggesting that between 6 and 5 ka, the sea level was ~1 m higher than the present along coastal Saurashtra. Compared to coastal Saurashtra, the Holocene sea-level studies from the tectonically active Kachchh coastline (Bhattacharya et al., 2014, 2019) are limited and also lack robust estimates from a common datum. Gupta (1975) suggested ~4-m-deep water at ~2 ka in the Little Rann. According to Khonde et al. (2011), marine sedimentation continued in the Great Rann until 1500 AD. In contrast, Tyagi et al. (2012) suggested that the western Great Rann was under the influence of tidal-flat sedimentation between 5.5 and 2 ka. Recently, Das et al. (2017) estimated ~2-m-high sea level between 6 and 3 ka from the Gulf of Kachchh. These studies

indicate that RSL fluctuated significantly and that, in addition to eustasy, hydro-isostasy (Banerjee, 2000), tectonic upliftment (Pant and Juyal, 1993; Juyal et al., 1995; Banerji et al., 2015), coastal configuration modifications, and sediment deposition by alongshore current near the Indus delta (Ferrier et al., 2015) are considered important.

Holocene sea level influenced and helped sustain coastal communities and contemporary human civilizations (Stanley and Warne, 1997; Day et al., 2007; Lawler, 2011). Particularly, the decrease in Mid-Holocene sea level enabled some populations to exploit the exposed coastal lowland environments for sustenance, human migration, and trade (Stanley and Warne, 1997; Fleming et al., 1998). This led to the suggestion of a possible link between the sea-level changes and contemporary human events (e.g., Stanley and Warne, 1997; Kennett et al., 2007). In the Indian context, the western Indian coastal Bronze Age Harappan (Indus Valley) settlements yielded artifacts like circular Persian Gulf seals, terracotta mummy-like figures, and fragments of greenish-gray stone (chlorite-schist) vessels bearing engraved geometric patterns suggesting cultural contact with the Persian Gulf via a sea route (Rao, 2000; Rawat, 2015) during the Mid-Holocene. Similarly, a circular seal bearing the Indus script from Madinat Hamad in Oman (Srivastava, 1991) and a Harappan black-slipped jar were recovered from coastal sites in Oman (Ajithprasad, 2006) suggesting sea trade and exchange of exotic items during Harappan times (Rawat, 2015). Gujarat has around 40 coastal Harappan sites, of which 30 correspond

to the mature urban period and 10 correspond to the late- or post-urban period. Of these 40 sites, 19 are along the coast of Kachchh (including Rann), which makes the area an ideal location for exploring the influence (if any) of Mid-Holocene sea level on the evolution of coastal Harappan settlements.

The present study thus aims to determine the RSL—the change in sea level relative to land at a particular time and site (Shennan, 2015)—from intertidal deposits using multiproxy data (sedimentology, trace elements, organic geochemistry, ichnology, and pollen) supported by optical and radiocarbon dating. The objectives are (i) to ascertain the magnitude and causes of Mid- to Late Holocene RSL changes, and (ii) to assess the influence of Mid- to Late Holocene RSL changes on coastal Harappan settlements.

STUDY AREA

The tectonically active nature of the Kachchh Peninsula is demonstrated by episodic high-magnitude intraplate earthquakes, such as the 1819 Allah Bund earthquake (M_w 7.8), the 1956 Anjar earthquake (M_w 6.1), and the 2001 Bhuj earthquake (M_w 7.6) (Rajendran and Rajendran, 2002; Mandal et al., 2004). It is traversed by east–west trending main faults that are transected by several younger oblique faults (Biswas, 2016) (Fig. 1B).

In this study we investigated RSL at three sites; two are located in estuaries (Kharod and Nani Cher) and one is at the distal end of Kori Creek. In the Kharod Estuary (Site-1, located ~200 km east of the Indus delta), two sections (1a and b) have been documented. The Kharod River originates in the southern Katrol Hill Range (KHR) and flows southward for ~60 km before meeting the Gulf of Kachchh (see Figs. 1B and 2A). The river flows through Mesozoic sandstone/limestone/shale, late Cretaceous Deccan basalt, and Tertiary sandstone/shale/laterite and limestone (Maurya et al., 2003). The India Bridge (INB, Site-2) is located at the northern terminus of the linear trench zone (Roy and Merh, 1982) (see Figs. 1B and 2B) and is considered as the farthest relict inland extension of Kori Creek. The rocky Mesozoic hills of Kunwar Bet flank it in the west, and the piedmont zone of Chappar Bet is in the east. Additionally, for broader spatial coverage, an archaeological mound near Nani Cher Estuary (Site-3), at the eastern flank of Kori Creek and ~70 km east of the Indus delta, is also explored. It is inundated during high tides (see Figs. 1B and 2C).

Geomorphological settings

In a tide-dominated coastline like the Gulf of Kachchh, a typical tidal-flat profile in the landward direction consists of a lower intertidal sand flat, a middle intertidal mixed sand-mud flat, and an upper intertidal mudflat (Desjardins et al., 2012). The relict intertidal flats are preserved in the spit-sheltered location of the tide-dominated Kharod Estuary and the distal end of the gourd-shaped Kori Creek. Such sheltered locations

with low tidal amplitudes and restricted wave activity are known to have fine, cohesive deposits from low-energy environments (weak current) and to facilitate gradual deposition of suspended material (Häntzschel, 1955; Lambeck et al., 2010). The absence of lamination further indicates intertidal sedimentation under slackened water conditions during low tidal waters (Semeniuk, 2005; Wang, 2012; Daidu et al., 2013). The alongshore current is from the west (Indus delta) to east (Gulf of Kachchh) and is responsible for the dispersion of suspended sediment in the Gulf of Kachchh (see Fig. 1B) (Ramaswamy et al., 2007).

Geomorphologically, the funnel-mouth estuary setting of the Kharod River is located in a spit and cusped foreland complex (Kar, 1993). In the estuarine zone, dissected southwest–northeast trending coastal dune (beach) ridges are preserved, whereas relict incised mudflats overlying the fluvial sediments form a conspicuous tableland topography (see Fig. 2, Site-1b). It is a mesotidal zone with an average high tidal range of ~2.70 m and an average low tide of ~0.90 m (Unnikrishnan et al., 1999; Vethamony and Babu, 2010). The modern and relict mudflats in the inner estuary flank the main channel axis.

The linear trench zone, in the vicinity of Site-2 (see Fig. 2), experiences spatial and temporal variability in the magnitude and extent of tidal inundation. For example, the southwestern part that lies close to Kori Creek is perennially under tidal inundation; the central part gets inundated during high tide, whereas the northeastern part around the Mesozoic rock-dominated Kunwar Bet gets flooded only during the exceptionally high monsoon wind-driven tidal surges (Glennie and Evans, 1976; Roy and Merh, 1982; Tyagi et al., 2012).

METHODOLOGY

The sedimentary sequences were documented and sampled to infer different depositional environments. Samples from units suggesting transitional depositional environments were chosen for geochemical and palynological analyses. Additionally, the intertidal deposits, which are used as sea-level indicators and index points (SLIPs), are characterized using multiproxy data.

Stratigraphy and sedimentology

At Site-1 (eastern flank of the Kharod River), two sections were excavated: the *Kharod Estuary section* (Site-1a) at the estuary mouth, and the *Kharod fluvial section* (Site-1b) located ~1 km further inland (see Fig. 2B). At the India Bridge (INB) section (Site-2), the stratigraphy was reconstructed from a trench after excavating through an elevated sandy mound (locally known as sandy Bet) and the Rann surface (see Fig. 2B). At Site-3, the *Nani Cher archaeological mound* was excavated on the left bank of the Nani Cher Estuary (see Fig. 2C). Data were collected describing sediment composition, texture (grain size), structures, and trace fossils in the measured units. All the elevations of the modern tidal-flat surfaces and studied sections were measured using

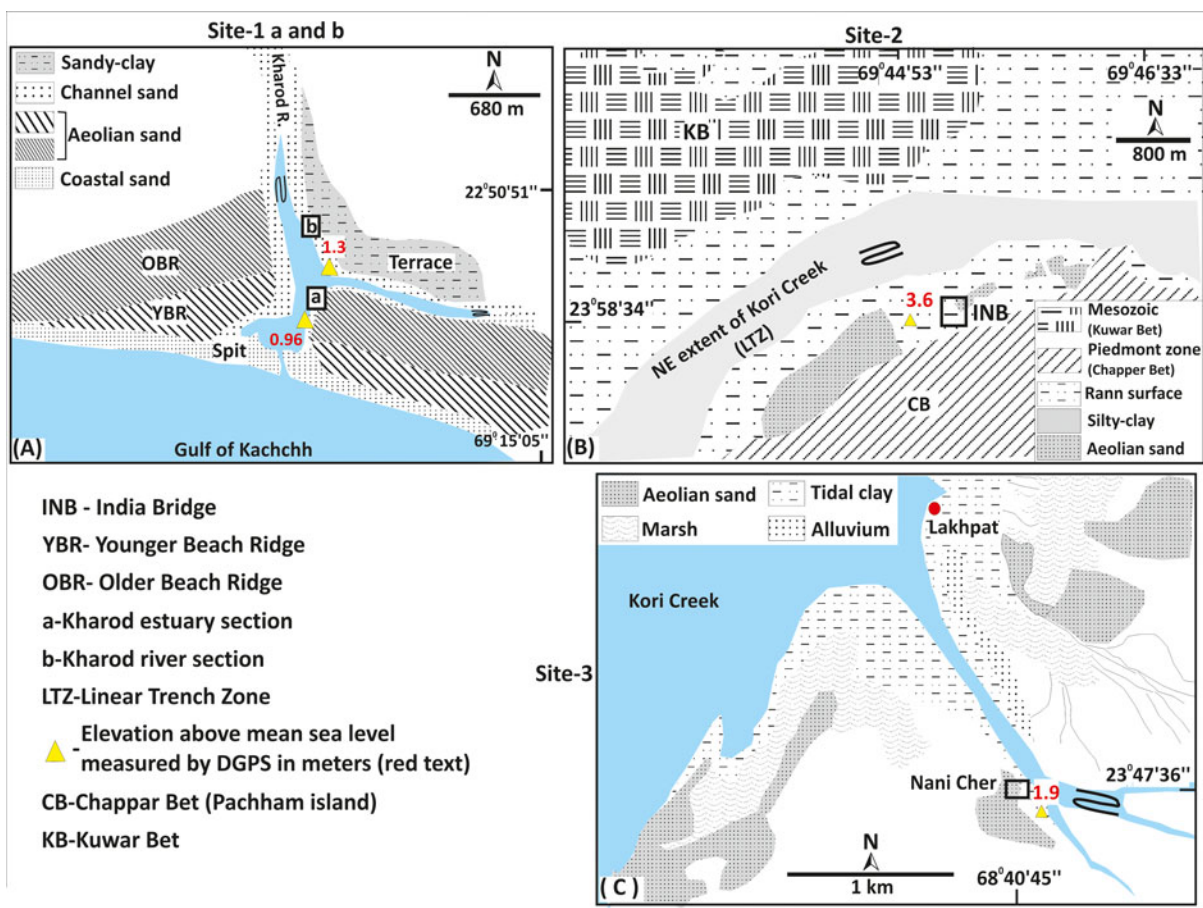


Figure 2. (color online) Geomorphological maps of Site-1a (Kharod Estuary section), Site-1b (Kharod River section), Site-2 (Indian Bridge), and Site-3 (Nani Cher).

differential global positioning system (DGPS) with an accuracy of ± 0.01 m. The cross-sectional profiles were made using Total Station with an accuracy of ± 0.03 m.

Grain size analysis was done on Sites 1 and 2 for sandy horizons to support field-based sedimentological observations and to characterize different depositional environments. Samples were dry sieved in a Retsch sieve shaker to obtain various size fractions. The statistical parameters (mean grain size, sorting, kurtosis, and skewness) were computed using the GRADISTAT program (Supplementary Table S1). From the INB section (Site-2), 9 samples from units-III and -IV and 10 samples (except pebbly sandy unit-I) from the Kharod Estuary section were analyzed for grain size.

Carbon, nitrogen, and C/N ratios analyses

The C_{org} and C/N ratio in tidal-flat/estuarine sediments are governed by the autochthonous (indigenous plants) and allochthonous contributions from the river catchment (Sampei et al., 1997; Allen et al., 2007). To characterize and differentiate between the tidal and fluvial environments, 21 samples (U-II and -III) from the Kharod Estuary section (Site-1a), 7 samples from the Kharod River section

(U-IV and -V, Site-1b), and 24 samples from INB section (U-I to -IV, Site-2) were analyzed using a Thermo Scientific Flash 2000 Elemental Analyser. The standards used for calibration were low organic content soil containing 1.65% carbon and 0.14% nitrogen. Higher C/N ratios in the tidal-flat environment suggest an increased proportion of river-imported detritus, and lower C/N ratios suggest proportionately more algae and less organic material from fluvial/terrestrial sources (Allen et al., 2007). Also, plants in general have higher C/N ratios than animals due to their low protein and high cellulose content. Therefore, the autochthonous component contributed by aquatic organisms, algae, and phytoplankton has a C/N ratio ranging from 4 to 10. The allochthonous constituent (mostly coming from terrestrial plants) is more refractory due to their high lignin and cellulose content and has a C/N ratio > 12 (Ku et al., 2005; Nazneen and Raju, 2017).

Geochemical analysis

The trace element geochemistry, including rare earth elements (REEs), is used to ascertain temporal changes in the sediment provenance (McLennan, 1993). In total, 28 samples from the Kharod Estuary section (Site-1a, unit-II [9 samples] and unit-III

[12 samples]), and Kharod River section (Site-1b, unit-V [7 samples]) were analyzed. In addition, modern intertidal sediments and Kharod River catchment lithology (basalt and sandstone) were also analyzed for comparison with the relict sediment.

Samples were washed in deionized water to remove the salt and were powdered using a planetary ball mill. Following this, the samples were treated with 10% HCl to remove the carbonate. Samples of approximately 300 mg each were digested using Savillex Teflon vials with ultra-pure HF-HNO₃ acids in a microwave-assisted digestion system. The final solutions were prepared in 2% HNO₃ acid. The analysis was done following the standard protocol in an inductively coupled plasma-mass spectrometry model iCAP-Q from Thermofisher (Ray and Shukla, 2018). The U.S. Geological Survey geological rock standard BHVO-2 was used for generating the calibration curves, and a laboratory standard (NOVA) was used as the unknown standard. A reproducibility check for trace elements was performed on repeated analyses on a different set of aliquots of BHVO-2 standard, which is better than 3% at the 2-sigma level.

The trace-element data, including REEs, were normalized with the upper continental crust composition (Taylor and McLennan, 1985). To ascertain probable sediment contribution into the Kharod Estuary, the geochemical data are compared with the Kharod River catchment dominant basalt lithology, modern intertidal sediments, and the Indus Delta sediments from Keti Bunder (Clift et al., 2010).

Trace fossils (ichnology) and palynological analysis

To further understand the nature of the depositional environment, the excavated sediment sections were investigated for trace fossils. The centimeter-scale, serial sectioning technique was used to identify trace fossil morphology following Häntzschel (1975) and Knaust (2017). Documented trace fossils were mostly vertical to sub-horizontal, with higher clay content. In order to ascertain the precise nature of the depositional environment, the trace fossil data are compared with the modern analog of the site—the proximal Mandvi intertidal zone (Patel and Desai, 2009).

For the palynological study, 10 samples from unit-III of the Kharod Estuary section (Site-1a), 4 samples from unit-V of the Kharod River section (Site-1b), and 4 samples from unit-I of the INB section (Site-2) were collected. The Nani Cher section (Site-3) is dominated by the sand fraction, and therefore it was not used for palynological study. Sediment samples of about 10 g were prepared following standard pollen analytical techniques, including acetolysis (Erdtman, 1943). Sample residues were mounted on microscope slides in a glycerine jelly medium. Pollen grains and fern spores were identified to the lowest possible taxonomic level using the Birbal Sahni Institute of Palaeosciences museum collection of reference pollen and published pollen keys (Thanikaimoni, 1987; Nayar, 1990). The pollen counts were made with the help of an Olympus microscope at a magnification of 400×. Most of the pollen samples were counted to a minimum of 150 grains.

CHRONOLOGY

Twelve samples were dated using the optically stimulated luminescence (OSL) technique. The OSL dating technique exploits the radiation dosimetric properties of mineral grains (usually quartz and feldspar). The energy from natural radioisotopes in the sediment is absorbed and stored in the crystal lattice of minerals that may be released as luminescence upon excitation/heating. It relies on the premise that the geological luminescence of samples is bleached to near residual levels during transportation and begins to accumulate once the sediment is deposited (Aitken, 1998). The samples were collected in specially designed opaque metal pipes, and the pure quartz was extracted by sequential pre-treatment with 10% HCl and 30% H₂O₂, respectively. The dried samples were sieved to obtain a 90–150 μm size fraction. Additionally, the quartz grains were checked for feldspar contamination by subjecting them to infrared stimulated luminescence (IRSL). The equivalent doses (De) were measured using a modified (double) single aliquot regeneration protocol (SAR; Murray and Wintle, 2000; Banerjee et al., 2001) except for two samples for which the RSL count was near background and the SAR protocol was used (Murray and Wintle, 2000). The luminescence measurements of the quartz extract were carried out in an automated Risø TL-OSL reader (TL/OSL-DA-20; Bøtter-Jensen et al., 2010). The samples were stimulated using a blue diode (470 ± 20 nm) and detected with an EMI 9835 QA photomultiplier tube coupled with a 7.5-mm Hoya U-340 filter (emission 330 ± 35 nm). An on-plate ⁹⁰Sr/⁹⁰Y beta source was used for beta irradiations. Typically, around 90 aliquots were analyzed, out of which 16–47 aliquots satisfied the criterion of a recycling ratio of 0.90–1.1 and were used for computing the De values. The growth curve, IRSL, shine down curve, and abanico plots showing the De distribution of each dated sample is given in the supplementary data (Supplementary Figs. S1–S3). For radioactivity, the concentrations of uranium, thorium, and potassium were measured in the high purity germanium detector (HPGe). The samples were sealed in plastic boxes and kept for ~15 days to attain radioactive equilibrium. The concentrations were estimated based on the characteristic gamma rays using a standard basalt reference source (107). The errors of measurement (systematic and statistical uncertainties) are <5% (Shukla et al., 2002). The appropriate statistical model, such as the Central Age Model (CAM) or the Minimum Age Models (MAM)-3/4, are chosen for the computation of De that is based upon the statistical parameters like over-dispersion (OD), skewness, and kurtosis (Bailey and Arnold, 2006; Galbraith and Roberts, 2012). The CAM is preferred if the OD is ≤40%, where OD as a criterion is usually sufficient to choose between CAM and MAM (Bailey and Arnold, 2006). This further suggests that sediments were adequately bleached (Galbraith and Roberts, 2012). Following the same criteria, we employed CAM for the computation of De values in R (calc_Central Dose) using the script of Burow (2019). The ages were computed using the java-based dose rate and age calculator (DRAC), which also

calculates the contribution from cosmic rays at a given location (Durcan et al., 2015). An average water content of $10 \pm 5\%$ was used (Fuchs et al., 2014).

In addition to this, two carbonate intertidal shell samples were radiocarbon dated and the radiocarbon activity was measured in a liquid scintillation counter “LKB-QUANTULUS” (Yadava and Ramesh, 1999). The samples were collected from the same horizons, which were also optically dated so that ages may be corroborated for consistency and reliability. Furthermore, it has been observed that the dead carbon effect (continental contamination) is expected to be minimal as the shells are collected from intertidal deposits with no restriction in water circulation (Hogg et al., 1998; Bezerra et al., 2000). The radiocarbon ages were calibrated using the Calib7.1.0 program and the Marine13 data set (Stuiver and Reimer, 1993; Reimer et al., 2013). The average marine reservoir age ($\Delta R \pm \sigma$ 135 ± 86 years) of three proximal locations (map no. 606-Pirotan Island, 591-Port Okha, and 592-Dwarka) was taken for reservoir age correction (Bhushan et al., 1994; Dutta et al., 2001) in the Calib7.1.0 program.

Sea-Level Index Point (SLIP) and RSL change

RSL change is used to quantify the change in sea level at a particular time and site relative to a land-based reference frame of the present (Shennan, 2015; Rovere et al., 2016). Based on multiple proxies, the intertidal deposits are characterized as lower, middle, and upper intertidal deposits. The upper intertidal deposits are formed between Mean High Water Spring (MHWS) and Mean High Water Neap (MHWN); middle intertidal deposits are formed between Mean High Water Neap (MHWN) and Mean Low Water Neap (MLWN); and the lower intertidal deposits are formed between the Mean Low Water Neap (MLWN) and Mean Low Water Spring (MLWS) (Daidu et al., 2013).

For a sea-level indicator to be identified as a SLIP, it must have the following well-constrained attributes: location, age, indicative meaning, and tendency (Shennan, 2015; Vacchi et al., 2018). Where the data points (both terrestrial and marine) could not be compared directly with the past tide levels, we ascribed these as limiting data points (Shennan and Horton, 2002). We used in situ, well-dated, relict intertidal deposits as SLIPs to calculate RSL changes, where RSL change is the elevation difference of the SLIP with respect to its modern analog (Shennan, 2015). Here elevation (amsl) of the SLIP is denoted by (Es), and elevation of the modern analog with reference to a tidal level is called the Reference Water Level (RWL). The range over which RWL varies is known as the Indicative Range (IR). The RWL (amsl) was estimated by taking the mean of n points at three corresponding locations (Supplementary Tables S2–S4). The IR (amsl) is at a 95% confidence interval and 1.96 times the standard deviation (Shennan et al., 2015). As suggested by Hijma et al. (2015), the errors were calculated by taking into account the IR error, DGPS error, sampling unit thickness error, vertical exposure error, variance in RWL, and variance of SLIP elevation (see Supplementary Table S1).

The RSL change was calculated using the respective modern analogs (Table 1) using statistically computed IR (see Supplementary Table S1). For comparison, the RSL was also estimated using IR determined from the various tidal ranges available at Okha tidal gauge station (see Fig. 1, Table 2), because the site proximal stations (Mandavi and Jhakau) have no record of MLWS, MHWS, MHWN, and MLWN (see Table 2). The absolute RSL values vary within the error limits (see Table 1), and hence we used the statistical IR for RSL estimation.

RESULTS

Stratigraphy

Site-1a (Kharod Estuary section, 22.845093°N, 69.229249°E)

An ~6-m-thick sediment sequence is exposed along the left flank of the tidal creek (see Figs. 2A, 3C, and 4). The elevation of the modern tidal surface is 0.96 m amsl. Based on the sediment texture and degree of weathering, five sedimentary units have been identified (see Fig. 4). The lowermost ~30-cm-thick unit-I is composed of faintly cross-laminated, angular to sub-rounded, pebbly quartz-rich, reddish-yellow sand containing subordinate basalt fragments and rolled calcrites. This is followed by the ~40-cm-thick unit-II, which contains pebbly sand mixed with subordinate (translocated) clay coating and angular to sub-rounded calcrite. Overlying this is the ~75-cm-thick unit-III of which the lower 35 cm is massive, compact, and weathered clayey-sand and the upper 40 cm is a sandy horizon that contains trace fossils (see Fig. 4A). Grain-size analysis shows the dominance of poorly sorted fine sand that is fine (positively) skewed (see Supplementary Table S1). The trace fossils include *Ophiomorpha nodosa*, *Polykladichnus* isp., *Planolites* isp, *Skolithos* isp, and a mud-lined burrow (see Fig. 4A). This is succeeded by the ~250-cm-thick unit-IV, which is compact, coarse, biogenic sand containing mica and randomly dispersed friable, tubular calcrites whose concentration increases upwards. Grain-size analysis shows the dominance of fine, moderately well to moderately sorted and finely skewed sand (see Supplementary Table S1). The ~200-cm-thick unit-V, which is micaceous, biogenic sand with insignificant friable calcrite concretions, overlies this unit (see Fig. 4). The grain size data indicate dominance of fine, moderately well-sorted and finely skewed sand that becomes very coarse (negatively) skewed to very finely skewed toward the top (see Supplementary Table S1).

Site-1b (Kharod River section, 22.857521°N, 69.228848°E)

An ~4.5-m-thick alluvial sequence is exposed along the left bank of the Kharod River (see Figs. 2A, 3B, and 5) where modern tidal flats are 1.3 m amsl. Based on the sediment texture and structures, five broad sedimentary units (base

Table 1. Details of intertidal deposits and the chronology that are used as SLIPS (Sea-Level Index Points). For comparison we give RSL estimates from two indicative ranges (IR1 and IR2) following the same protocol (for details see Supplementary Tables S1–S3). RSL1 is estimated using IR1, and RSL2 is estimated using IR2. As can be seen, the RSL does not vary significantly (it fluctuates within the errors). Average RSL values are calculated and corrected for tectonic component from RSL1. All values are in meters above mean sea level (m amsl). At the Kharod Estuary/river and IB sections the uplift rates are 0.13 ± 0.01 mm/yr and 0.2 ± 0.01 mm/yr, respectively.

S. No.	Section	Indicates	Modern analog	RWL	IR1	IR2	Es	RSL1t	RSL2t	RSL1	RSL2	Age
1	Kharod Estuary (lower intertidal)	MLWN to MLWS	Kharod Estuary mouth 0.96	0.96	0.15	0.79	2.38	1.42 ± 0.38	1.42 ± 0.55	0.51 ± 0.38	0.51 ± 0.55	7.3 ± 0.4 ka
2	Kharod River (middle intertidal)	MLWN to MHWN	Kharod Estuary inland 1.3	1.3	0.18	1.76	4.6	3.3 ± 0.53	3.3 ± 1.0	2.39 ± 0.53	2.39 ± 1.0	6.8 ± 0.5 ka
3	IB (upper intertidal)	MHWS to MHWN	Sunda High 2.1	2.1	0.28	0.51	2.8	0.73 ± 0.43	0.73 ± 0.48	0.53 ± 0.43	0.53 ± 0.48	1045 ± 175 cal yr BP, 1.1 ± 0.1 ka
Mid-Holocene average RSL without tectonic correction												
Mid-Holocene average RSL with tectonic correction												
Late-Holocene average RSL without tectonic correction												
Late-Holocene RSL with tectonic correction												

Notes: RWL = Reference Water Level; IR1 and IR2 = Indicative Ranges; Es = Elevation of the dated relic intertidal units top; RSL1t and RSL2t = Relative Sea-Level change with tectonic overprinting; RSL1 and RSL2 = Relative Sea-Level change without tectonic overprinting; MLWN = Mean Low Water Neap; MLWS = Mean Low Water Spring; MHWS = Mean High Water Spring; and MHWN = Mean High Water Neap.

unexposed) have been identified (see Fig. 5). From bottom upwards, unit-I (30 cm) is dominated by medium to fine friable sand containing dispersed calcretes. Unit-II contains ~40-cm-thick bedded calcretes with subordinate rolled calcrete nodules. This unit is weathered and laterally persistent along the river to a distance of ~500 m (see Fig. 3B). It is overlain by unit-III, which is ~100 cm thick and composed of cross-stratified (planar and trough) calcrete gravel. The bedding attitude (azimuths) of the cross-stratification exhibits strike of east–west (90–270°) to east-southeast–west-northwest (95–275°) and dips gently toward the south (180°) to south-southwest (185°). The overlying ~200-cm-thick unit-IV contains crudely stratified rounded to sub-rounded calcrete gravels, subordinate basalt lithoclasts, and impersistent sand lenses. The uppermost 75-cm-thick unit-V is dominated by weathered dark brown massive and fractured sandy-clay with a sharp basal contact (see Fig. 5), which forms a well-defined terrace surface around the Kharod Estuary (see Fig. 2A).

Site-2 (India Bridge section, 23.977750°N, 69.757433°E)

This site is located ~70 km inland in the distal linear trench zone of Kori Creek (Gulf of Kachchh) and is 3.6 m amsl (see Figs. 1 and 2C). The stratigraphy is reconstructed from an ~3-m-deep trench excavated at the western margin of Chappar Bet (see Figs. 3E and 6). The lowermost 30-cm-thick unit-I is composed of dark gray sticky clay containing gastropod shells (*Melania striatella tuberculata*). This is followed by 60 cm of thick clayey-sand containing shells and bioclast fragments (unit-II). The sticky clay is gradually replaced by medium to fine silty-sand in the upper part. The overlying ~70-cm-thick unit-III is dominated by poorly to moderately sorted fine sand that is coarsely skewed toward the top (see Supplementary Table S1). The uppermost ~125-cm-thick unit-IV is massive fine to very fine moderately well-sorted sand (see Supplementary Table S1) containing bioclast fragments (see Fig. 6). The sandy units are devoid of mica.

Site-3 (Nani Cher Archaeological mound, 23.795944°N, 68.678600°E)

The archaeological mound with underlying alluvium is excavated along the eastern flank of the Nani Cher Estuary (see Fig. 2C) in which three broad stratigraphic units were identified (Fig. 7). The modern tidal flat is 1.9 m amsl at this location. From bottom upwards, the lowermost ~300-cm-thick unit-I is dominated by pebbly-coarse sand containing occasional charcoal and potsherds. Unit-I continues below the modern tidal flat that abuts it (see Fig. 7). This is overlain by the ~400-cm-thick unit-II, which is dominated by randomly dispersed archaeological deposits such as iron slag, ash layers, potsherds, bones, shells, and bangles. At places, the unit is punctuated by channel activity, which is represented by lenticular sand layers overlain by clayey-silt. The archaeological

Table 2. Tide gauge data recorded at the mouth of the Gulf of Kachchh near Okha (west and southwest of the studied sites) (Babu et al., 2005), Mandavi (near Kharod Estuary), and Jakahu port near Kori Creek (Gujarat Maritime Board).

Gauge station	MHWS	MHWN	MLWN	MLWS	MSL	HHW	MHHW	MLHW	MHLW	MLLW
Okha	3.47	2.96	1.20	0.41	2.00	–	–	–		
Jakahu	–	–	–	–	–	4.90	2.90	2.65		
Mandavi					2.59	4.80	4.06	3.65	1.66	1.00

Notes: MHWS = Mean High Water Spring, MHWN = Mean High Water Neap, MLWN = Mean Low Water Neap, MLWS = Mean Low Water Spring, MSL = Mean Sea Level, HHW = Higher High Water, MHHW = Mean Higher High Water, MLHW = Mean Low Higher Water, MHLW = Mean High Low Water, and MLLW = Mean Lower Low Water.

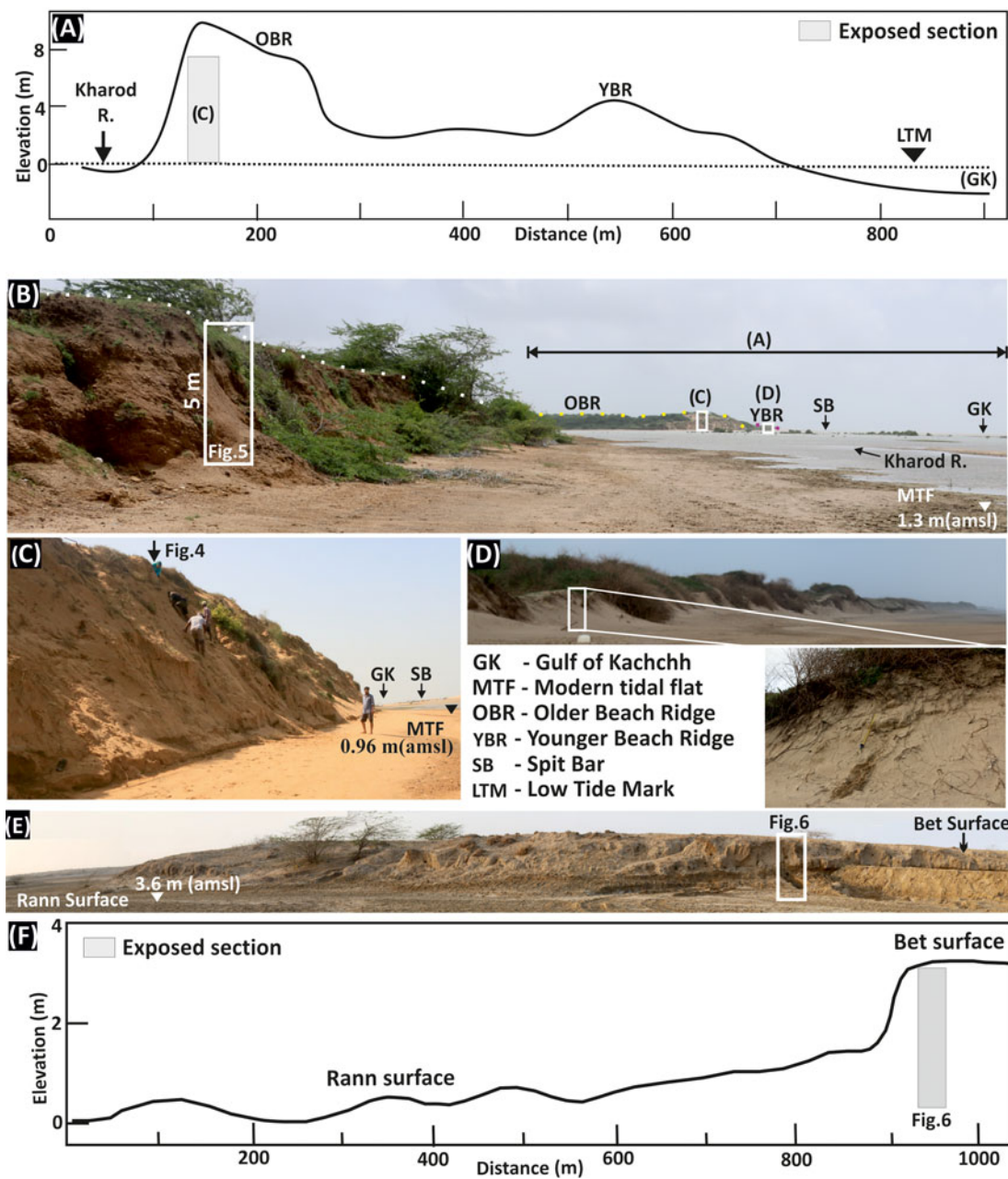


Figure 3. (color online) (A) Cross-section profile generated using Total Station survey data from the Gulf of Kachchh (GK) to the Kharod River section. Low tide mark (LTM) elevation as of April 7, 2017. (B) Field photograph showing locations of Kharod River and estuary sections (Site-1a and Site-1b). (C) Field photographs of the Kharod Estuary and (D) younger beach ridge (YBR) with close-up. (E)–(F) Field photos and cross-section profile at Site-2 near India Bridge.

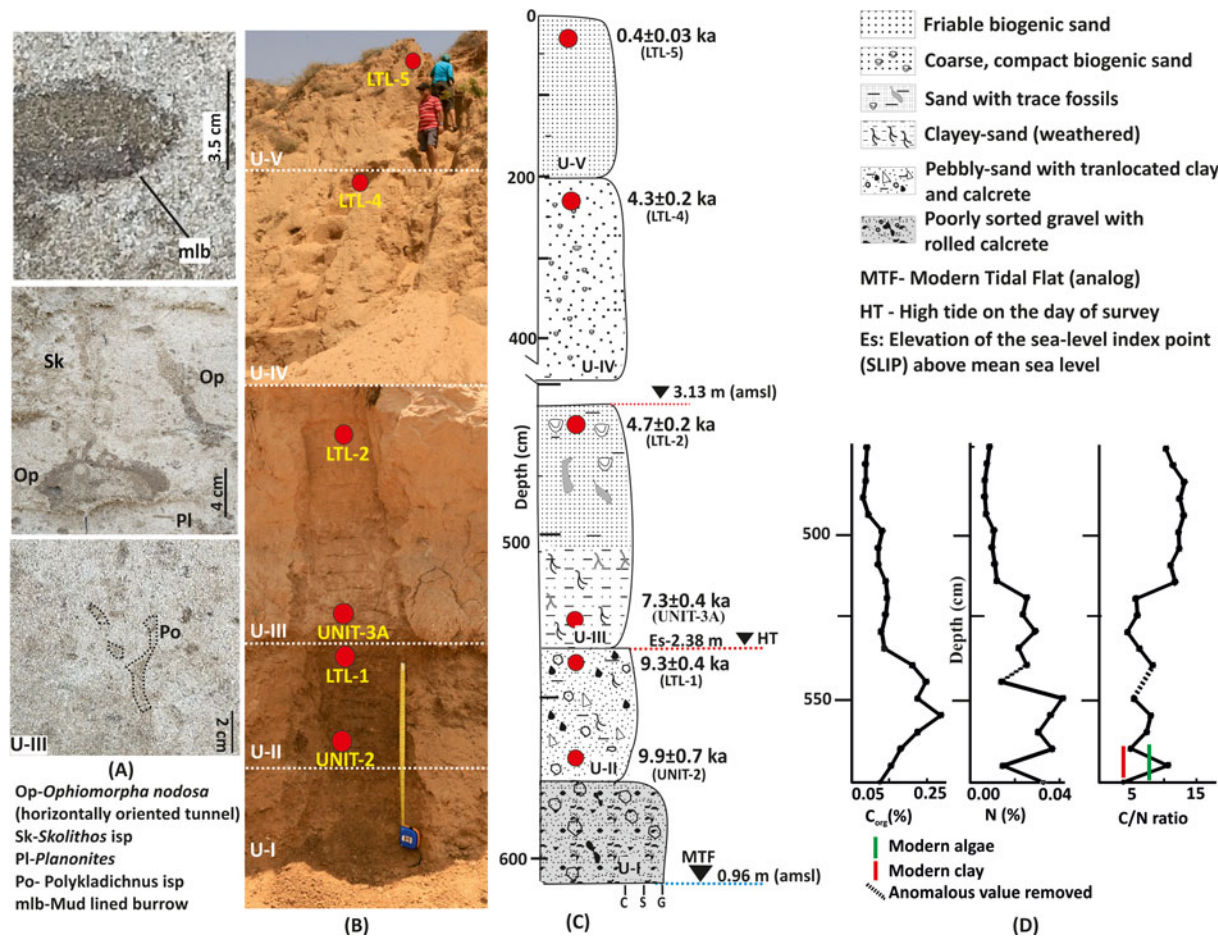


Figure 4. (A) Close-ups of trace fossils and mud-lined burrow (mlb), which are filled with passive sediments from the upper bioturbated section of unit-III. (B) Close-up of Kharod Estuary section with optically stimulated luminescence (OSL) sample locations (red circles). (C) The stratigraphic details along with the OSL ages. The average differential global positioning system (DGPS) elevation of the modern lower intertidal flat ($n = 30$) corresponds to Mean Low Water Spring (MLWS) and Mean Low Water Neap (MLWN) range. The high tide (HT) is the level of high tide marked on the day of survey (April). (D) C_{org} , N_{total} , and C/N ratio obtained on unit-II and -III indicate dominance of marine organic matter. (For interpretation of the references to color in this figure legend, the reader is referred to the web version of this article.)

mound is covered with the rubified aeolian sand (unit-III) (see Fig. 7).

Carbon_{org} (C_{org}), Nitrogen (N_{total}), and C/N ratios

In the Kharod Estuary section (Site-1a), the N_{total} and C_{org} has a declining trend toward the top, whereas the C/N ratio shows an increasing trend from mid-unit-III (see Fig. 4D, Supplementary Table S5). The C/N ratios for the modern clay and algae are 4.0 and 5.6, respectively (see Supplementary Table S5). In the Kharod River section (Site-1b), N_{total} shows an increasing and then decreasing trend, while the C_{org} is has an increasing trend. The C/N ratio preferentially increases toward the top (see Fig. 5C). In the INB (Site-2) section, N_{total} has its highest concentration at the bottom, C_{org} has its highest concentration in unit-I and its lowest concentration in unit-II and unit-IV, and the C/N ratio has an overall increasing trend toward the top (see Fig. 6C, Supplementary Table S5).

Trace elements geochemistry

For provenance interpretation, we used the average values of the trace element data that were generated from 21 samples from Site-1a (Kharod Estuary section, units-II and -III), 7 samples from Site-1b (Kharod River section, unit-V), modern intertidal sediments, and the catchment's dominant lithology samples (basalt and sandstone) (Fig. 8, Table 3).

Trace fossils and palynological evidence

The trace fossils *Ophiomorpha nodosa*, *Polykladichnus* isp., *Planolites* isp., and *Skolithos* isp. and mud-lined burrows (see Fig. 4) dominate unit-III in the Kharod Estuary section (Site-1a). *Ophiomorpha nodosa* occurs as a thick nodose walled burrow, elliptical in cross section, 14 cm in diameter and was made by a suspension-feeding trace maker like *Oratosquilla striata* (Patel and Desai, 2009). *Polykladichnus* isp. occurs as vertical to inclined Y-shaped burrow made by a suspension-feeding trace maker. *Planolites* isp. occurs as a

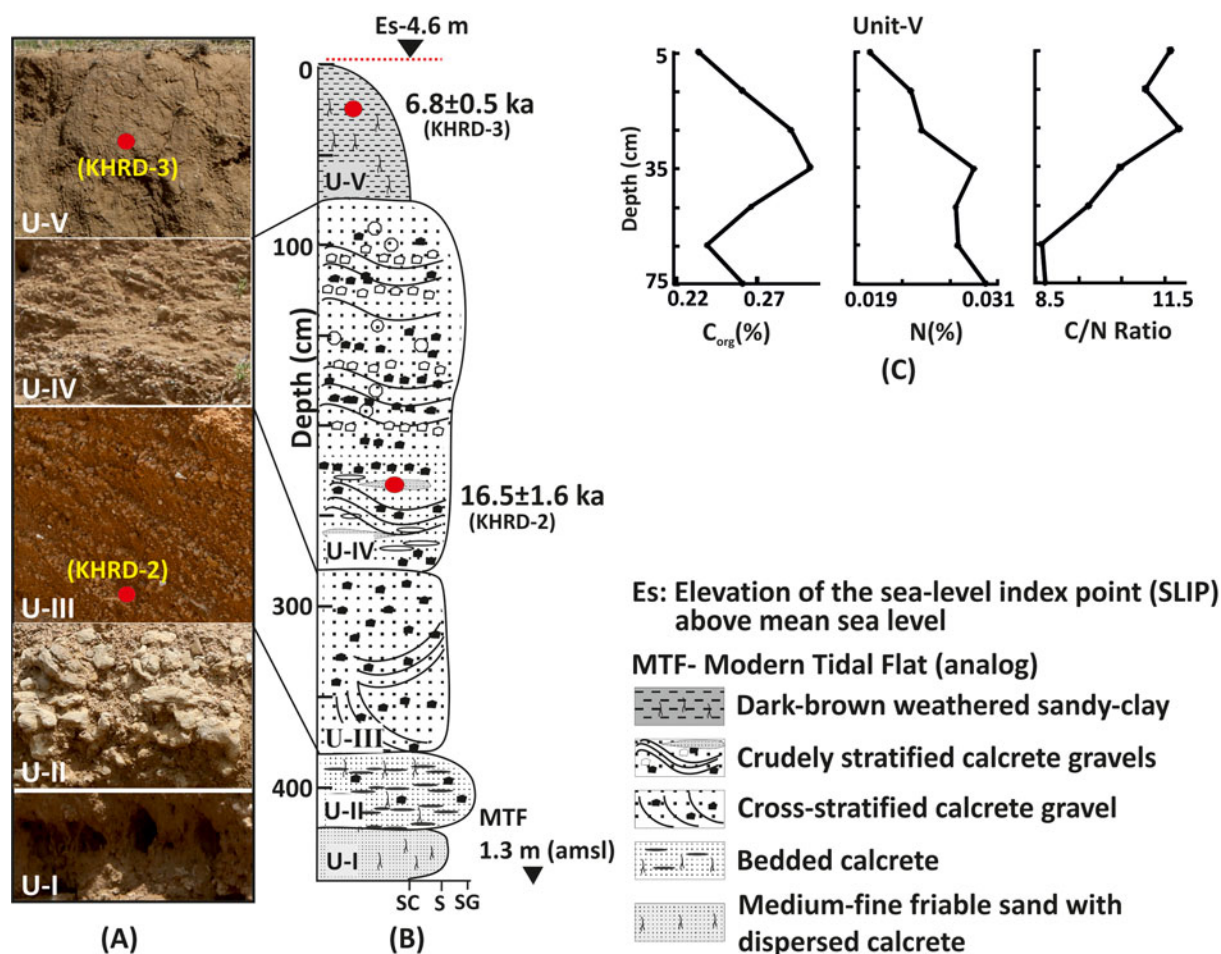


Figure 5. (A) Close-up field photographs of the Kharod River section with location of optically stimulated luminescence (OSL) samples (red circles). (B) Stratigraphic details along with the OSL ages. The average differential global positioning system (DGPS) elevation of the modern middle tidal flat ($n = 20$) corresponds to Mean Low Water Neap (MLWN) and Mean High Water Neap (MHWN). (C) C_{org} , N_{total} , and C/N ratio indicate dominance of marine organic matter. (For interpretation of the references to color in this figure legend, the reader is referred to the web version of this article.)

circular to elliptical cross section of the horizontal burrow with active burrow filling made by deposit-feeding trace makers. *Skolithos* isp. is a vertically oriented unbranched burrow of suspension-feeding trace makers (Patel and Desai, 2009). Many modern crustaceans commonly make mud-lined burrows by inserting pellets along burrow walls.

No pollen spores were recovered from the Kharod Estuary (Site-1a) unit-III except for a few fungal spores, which could be due to a higher concentration of sand. Also, there was no significant yield from the INB (Site-2) section. In contrast, the Kharod River section (Site-1b) unit-V yielded mangrove pollen taxa such as *Rhizophora mucronata* and *Avicennia marina*. The other mangrove pollens, including *Bruguiera* and *Ceriops*, were also present but in lower percentages. The lower part of this unit has a higher representation of *R. mucronata* (20–35%) and a high concentration of *Avicennia* (50%). Among the terrestrial taxa, pollen grains of Malvaceae, *Prosopis juliflora*, and Myrtaceae were recorded in low values. In general, herbs and grasses are consistently present throughout this unit at values ranging from 15% to

30%. The highest presence of herbs and grasses such as Asteraceae, Cyperaceae, *Artemisia*, Poaceae, and Chenopodiaceae/Amaranthaceae were observed in the upper portion.

Chronology

The fluvial sand facies with translocated tidal clay (unit-II) at the Kharod estuary section (Site-1a) is dated to 9.9 ± 0.7 ka (UNIT-2) and 9.3 ± 0.4 ka (LTL-1). The overlying intertidal unit-III is dated between 7.3 ± 0.4 ka (UNIT-3A) and 4.7 ± 0.2 ka (LTL-2). The upper aeolian beach ridge (unit-IV) is dated to 4.3 ± 0.2 ka (LTL-4), and unit-V is dated to 0.4 ± 0.03 ka (LTL-5) (see Fig. 4, Table 4). The younger (modern) beach ridge is dated to 0.2 ± 0.01 ka (MBR) (see Fig. 3D), which is located ~ 100 m from the modern shoreline and is ~ 3 m high. At Kharod fluvial section (Site-1b), the planar stratified gravelly sand (unit-IV) is dated to 16.5 ± 1.6 ka (KHRD-2), and the upper intertidal clay (unit-V) is dated to 6.8 ± 0.5 ka (KHRD-3) (see Fig. 5). At India Bridge (Site-2), the gastropod shell (*Melania stiatella tuberculata*) collected from the lowest

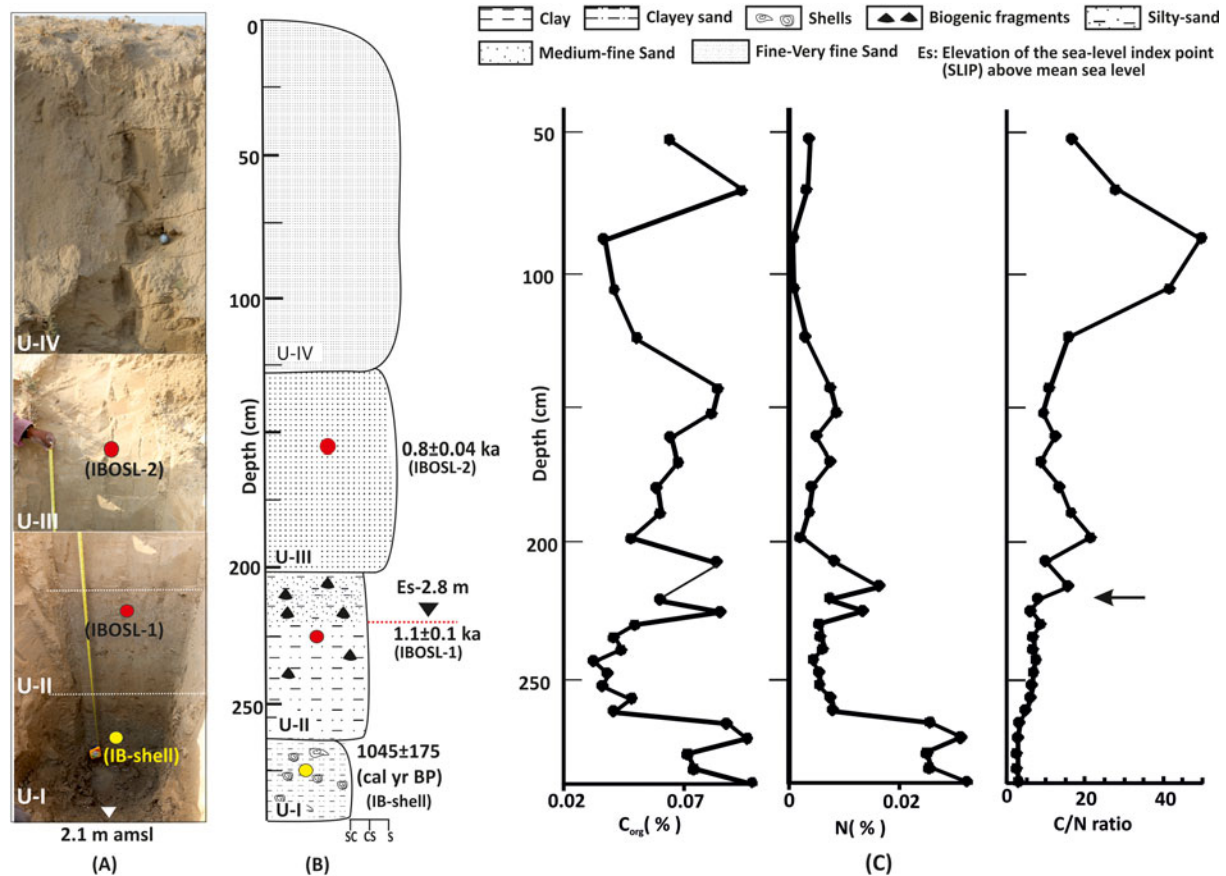


Figure 6. (A) Close-up field photograph of the India Bridge (INB) sediment profile, optically stimulated luminescence (OSL) samples (red circles), and radiocarbon locations samples (yellow circle). The average differential global positioning system (DGPS) elevation ($n = 6$) of the modern upper tidal flat at Sunda High (white inverted triangle) corresponds to Mean High Water Spring (MHWS) and Mean High Water Neap (MHWN) range. (B) Stratigraphy details along with the OSL ages. Es is also marked considering the low (marine) C/N ratio. (C) Note that units-I and -II showing low C_{org} , C/N ratio, and relatively high N_{total} suggesting deposition under a distal intertidal environment. Black arrow marks the break in trend (increased aeolian influence). (For interpretation of the references to color in this figure legend, the reader is referred to the web version of this article.)

unit-I is radiocarbon dated to 1045 ± 175 cal yr BP (IB-shell) (see Fig. 6, Table 5). The overlying unit-II is optically dated to 1.1 ± 0.1 ka (IBOSL-1), and the unit-III is dated to 0.8 ± 0.04 ka (IBOSL-2) (see Fig. 6). At Nani Cheri Estuary (Site-3) the *Turbinella Pyrum* (conch shell) is radiocarbon dated to 3210 ± 155 cal yr BP (Kld-shell) (see Fig. 7, Table 5), and a sandy layer in unit-II is optically dated to 2.9 ± 0.2 ka (KLARD-4). Details of the radioactivity, dose rate, equivalent dose, and the ages obtained are shown in Table 4, and typical growth curves, shine down and IRSL plots, and De distribution are given in Supplementary Figures S1–S3.

DISCUSSION

Depositional environment

Site-1a (Kharod Estuary section, $22.845093^{\circ}N$, $69.229249^{\circ}E$)

The lowermost faintly cross-laminated pebbly sandy unit-I can be interpreted as channel lag deposits (Therrien, 2006).

Because of the limited space of the river channel, the river repeats stages of erosion and accumulation in the adjacent regions. The overlying pebbly sand containing angular to sub-rounded calcrite with occasional clay coating (unit-II) suggests deposition under a relatively stable fluvial environment (consistent discharge with occasional flooding) (Juyal et al., 2000; Bhattacharya et al., 2014). The clay coating seems to be physically translocated from the overlying unit-III through cracks (see Fig. 4); this is suggested to be the reason for a relatively high concentration of organic carbon and nitrogen in unit-II because clay provides a large surface area and has a higher sorptive capacity (Dunn et al., 2008; Nazneen and Raju, 2017). The grain-size dependency for carbon and nitrogen is further supported by the modern clay sample from the Kharod estuary, which contains 0.90% C_{org} , 0.22% N_{total} , and a C/N ratio of 4. However, the C/N ratio (except for one point) remains below 10, implying that the organic matter and the nitrogen were largely contributed from marine sources (Bordovskiy, 1965; Prahl et al., 1980).

Considering the textural attributes of unit-III (clayey-sand), it can be suggested that it is an intertidal deposit

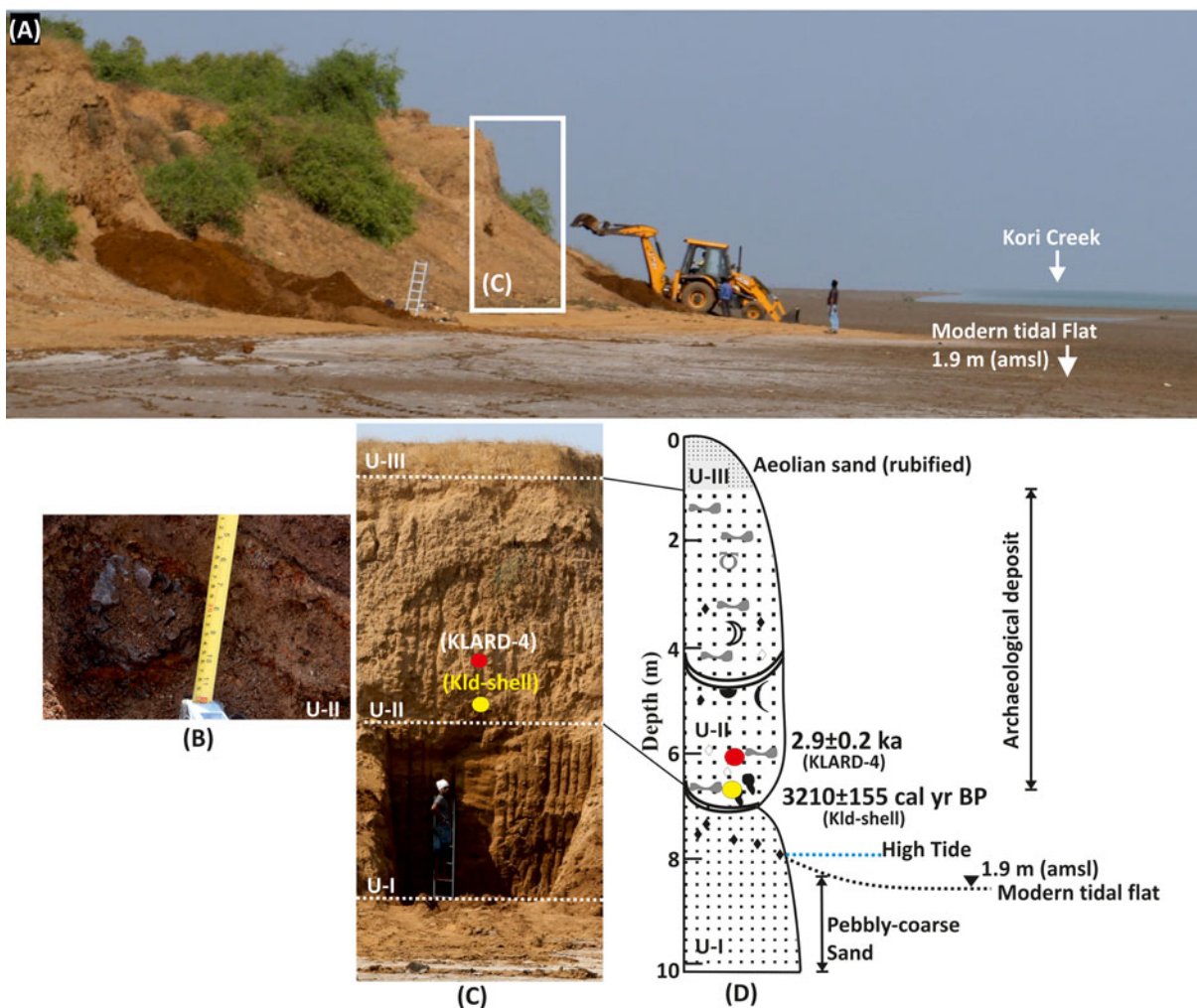


Figure 7. (A) Field photograph showing the panoramic view of Nani Cher Estuary, location of the section excavated is shown by a white rectangle. (B) Close-up of unit-II showing iron slag in archaeological deposit. (C) Field photograph and (D) stratigraphic details of the section. Note that unit-I continues below the modern intertidal flat. The radiocarbon age (yellow circle) of 3210 ± 155 cal yr BP (Kld-shell) is obtained on *Turbinella pyrum* (conch shell) collected ~ 60 cm above the high tide (HT) (May 2017), and the sediment sample (red circle) is dated to 2.9 ± 0.2 ka. (For interpretation of the references to color in this figure legend, the reader is referred to the web version of this article.)

where deposition occurred by a combination of tidal current (deposition of sand) followed by the slackening facilitating the deposition of clay as suspension fall out (Häntzschel, 1955). Further, the absence of lamination suggests sedimentation under a relatively low-energy, lower-intertidal environment (Semeniuk, 2005; Wang, 2012; Daidu et al., 2013) and not the subtidal environment that is dominated by coarser sediment having lag-scour structures produced by lateral migration of bedforms under subtidal high energy currents (Dalrymple et al., 2012; Daidu et al., 2013). The possibility of post-depositional erosion is negated, because unit-III can be laterally traced (~ 1 km toward the coast) with near-uniform thickness and is overlain by aeolian sand (older beach ridge and reworked deposits). Unit-III also has a moderate Bioturbation Index of BI-3 made up of high-density mud-lined burrows of suspension-feeding organisms (e.g., *Ophiomorpha nodosa*). Construction of mud-lined burrows requires organisms to extract mud from

suspension mode and use it to support its burrow walls. In contrast, organisms with deposit feeding will recycle and process the sediment and deposit it as an active burrow fill, thus generating an entirely different morphology of trace fossil. Thus, for the survival of suspension-feeding organisms, water is required to be under agitated conditions to keep the mud and organic matter in suspension mode—a condition usually found in the lower intertidal/subtidal zone (more frequently toward the low water line) (Desai and Patel, 2008; Dalrymple et al., 2012). Moreover, the *Ophiomorpha* burrows are absent near the high-tide level/foreshore/backshore area, as the trace maker cannot sustain the environmental stress-induced prolonged exposure between the tides along with heat and lack of water. Similar occurrence of *Ophiomorpha* from lower intertidal and subtidal zones are also persistent from the Pleistocene-age Dwarka Formation exposed along the southern shores of the Gulf of Kachchh (Desai, 2016), and from modern lower

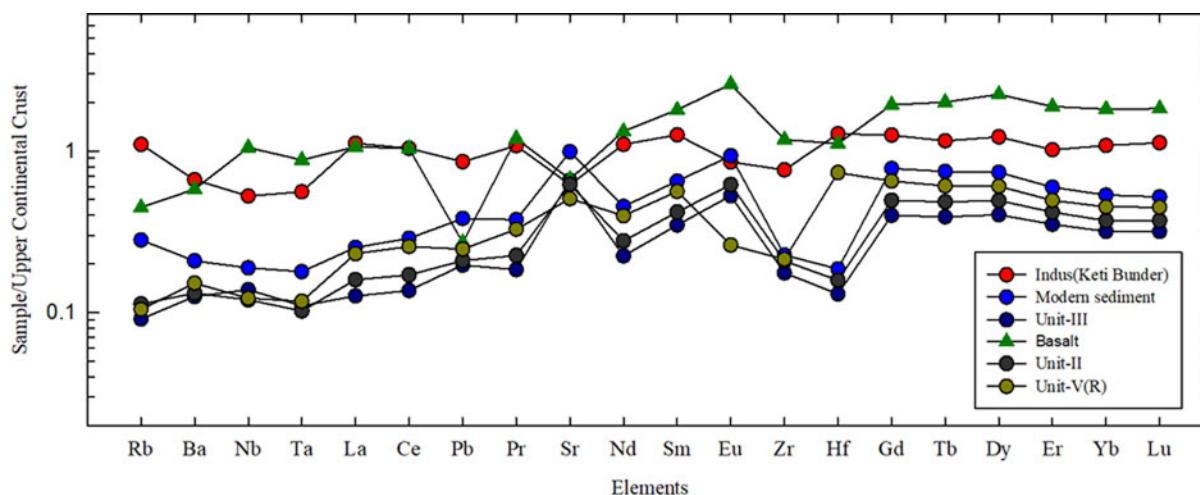


Figure 8. (color online) The plot of upper continental Crust (UCC) (Taylor and McLennan, 1985) normalized trace elements from the Kharod Estuary section (units-II and -III), Kharod River section (unit-V), and modern tidal clay. The normalized trace element values of Kharod River catchment lithology (basalt) and the Indus delta sediments (Keti Bunder; Clift et al., 2010) are also shown.

intertidal/ subtidal zones along Mandvi to Mundra in the northern shores of the Gulf of Kachchh (Desai and Patel, 2008; Patel and Desai, 2009). Additionally, the ichnozonation model of the tide-dominated depositional profile of Buatois and Mângano, (2011, p. 142) also supports higher/moderate trace fossil diversity and degree of bioturbation in the lower intertidal zone, which decreases significantly in the subtidal zone owing to widespread high energy conditions and scouring (Buatois and Mângano, 2011, p. 142). Thus, ichnological diversity and density with BI-3 along with the sedimentological evidence suggests that unit-III was deposited under lower intertidal zone deposits between MLWS and MLWN (Daidu et al., 2013).

The overlying, moderately compact well-sorted, very coarse to very finely skewed fine sand corresponding to unit-IV and -V having a variable concentration of broken shell fragments, indicate transportation by winds from near coastal environments (source proximal). The overlying

coarse to moderately skewed fine sand with dispersed broken shells suggests sub-recent accretion by coastal winds and deposition as linear hummocky mounds, similar to the coastal dunes/beach ridges in a prograding coastline (Compton and Franceschini, 2005). Johnson (1919), was the first to describe beach ridges in the geological literature and considered these to be constructed by waves along successive shore positions. The beach ridges are narrow, sub-parallel, relict fore dunes of strand plains (Otvos, 2000). These are formed by a combination of waves and winds in areas having an abundance of sediment supply with low offshore gradient and can be used to reconstruct RSL (Taylor and Stone, 1996). The typical morphology is ascribed to vegetation that forms at the upper limit of swash, and the ridge growth is accomplished by aeolian deposition (Hesp, 1984). The beach ridges thus are defined as relict, semi-parallel, multiple wave- and wind-built landforms that originated in the inter- and supra-tidal zones. It is suggested that since the

Table 3. Average values of trace element concentrations from dominant lithology, modern intertidal sediments, and different sedimentary units plotted in Figure 8 are given. The range of concentration is given in parentheses.

Trace elements (ppm)	Modern intertidal clay		Kharod Estuary section (Site-1a)		Kharod River section (Site-1b)
	Basalt	Sandstone	Unit-II	Unit-III	Unit-V
Rb (ppm)	50.1	25.3	12.6 (10.6–14.4)	10.2 (6.37–12.7)	11.7 (10.6–12.8)
Ba	319.0	365.0	72.5 (68.8–75.7)	69.1 (54.4–78.6)	83.5 (75.7–95.4)
Th	7.4	4.4	0.8 (0.69–1.11)	0.6 (0.46–0.82)	1.4 (1.20–2.00)
U	1.7	1.9	0.3 (0.29–0.39)	0.3 (0.22–0.82)	0.4 (0.40–0.46)
Nb	26.3	14.1	3.0 (2.47–3.24)	3.5 (2.92–4.48)	3.1 (2.90–3.50)
Ta	1.9	1.1	0.2 (0.17–0.35)	0.2 (0.19–0.39)	0.3 (0.20–0.45)
Pb	5.4	8.4	4.2 (3.85–4.57)	3.9 (3.23–4.54)	4.9 (4.7–5.49)
Zr	223.0	122.0	39.6 (29.1–52.5)	33.4 (16–44.2)	49.7 (44.4–62.7)
Hf	6.5	3.7	0.9 (0.69–1.20)	0.8 (0.33–1.04)	1.2 (1.10–1.38)
∑LREE	149.0	34.7	26.4 (22.8–36.6)	21.3 (16.2–29.9)	38.5 (34.7–46.9)
∑HREE	27.7	3.9	6.7 (5.84–8.06)	5.5 (3.83–7.04)	8.3 (7.65–9.02)

Table 4. Details of the samples, number of aliquots used (N), radioactivity details, over dispersion (OD), central age model (CAM) equivalent dose (De), dose rate, and ages obtained for various landforms. Water content used $10 \pm 5\%$ (Fuchs et al., 2014).

S. No.	Sample name and details	N	U (ppm)	TH (ppm)	K (%)	Rb (ppm)	OD (%)	CAM De (Gy)	Dose rate (Gy/ka)	Age (ka)
1.	LTL-1 22.845093°N, 69.229249°E, 6 m amsl Depth-400 cm	47	1.50 ± 0.05	7.59 ± 0.2	0.97 ± 0.02	48.5 ± 1.5	14	16.5 ± 0.4	1.8 ± 0.1	9.3 ± 0.4
2.	LTL-2 22.845093°N, 69.229249°E, 6 m amsl Depth-250 cm	47	1.49 ± 0.05	7.38 ± 0.2	0.78 ± 0.02	39 ± 1.5	15	7.6 ± 0.2	1.6 ± 0.2	4.7 ± 0.2
3.	LTL-4 22.845093°N, 69.229249°E, 6 m amsl Depth-50 cm	42	1.58 ± 0.06	7.33 ± 0.3	0.69 ± 0.02	34.5 ± 1.5	8	6.8 ± 0.1	1.6 ± 0.1	4.3 ± 0.2
4.	LTL-5 22.845093°N, 69.229249°E, 6 m amsl Depth-50 cm	26	1.38 ± 0.05	7.54 ± 0.2	0.70 ± 0.02	35 ± 1.5	11	0.7 ± 0.03	1.6 ± 0.1	0.4 ± 0.03
5.	IBOSL-1 23.977750°N, 69.757433°E, 43 m amsl Depth-200 cm	37	2.14 ± 0.05	10.4 ± 0.3	1.5 ± 0.02	75 ± 1	22	2.9 ± 0.1	2.6 ± 0.1	1.1 ± 0.1
6.	IBOSL-2 23.977750°N, 69.757433°E, 43 m amsl Depth-100 cm	19	1.88 ± 0.04	7.65 ± 0.2	1.5 ± 0.02	75 ± 1	13	1.8 ± 0.08	2.4 ± 0.1	0.8 ± 0.04
7.	KHRD-2 22.857521°N, 69.228848°E, 4.5 m amsl Depth-100 cm	16	1.72 ± 0.09	8.99 ± 0.4	1.52 ± 0.04	76 ± 2.5	36	40.8 ± 3.7	2.5 ± 0.1	16.5 ± 1.6
8.	KHRD-3 22.857521°N, 69.228848°E, 4.5 m amsl Depth-20 cm	18	1.24 ± 0.05	6.89 ± 0.3	1.5 ± 0.04	40 ± 1	23	15.4 ± 0.9	2.3 ± 0.1	6.8 ± 0.5
9.	UNIT-3A 22.845093°N, 69.229249°E, 6 m amsl Depth-200 cm	27	1.41 ± 0.04	7.73 ± 0.2	0.91 ± 0.02	59.5 ± 1	17	12.7 ± 0.5	1.7 ± 0.1	7.3 ± 0.4
10.	UNIT-2 22.845093°N, 69.229249°E, 6 m amsl Depth-200 cm	19	1.41 ± 0.04	7.73 ± 0.2	0.91 ± 0.02	59.5 ± 1	24	17.2 ± 1.0	1.7 ± 0.1	9.9 ± 0.7
11.	MBR 22.845093°N, 69.229249°E, 6 m amsl Depth-20 cm	24	1.04 ± 0.08	10.1 ± 0.5	0.37 ± 0.02	18.5 ± 1.5	29	0.3 ± 0.02	1.4 ± 0.1	0.2 ± 0.01
12.	KLARD-4 23.795944°N, 68.678600°E, 4 m amsl Depth-600 cm	24	2.20 ± 0.04	6.59 ± 0.2	0.77 ± 0.01	38.5 ± 0.5	16	4.9 ± 0.19	1.7 ± 0.1	2.9 ± 0.2

Mid-Holocene RSL, beach ridges prograded episodically seaward (Tankard and Rogers, 1978; Otvos, 2000). Thus, the presence of two distinct beach ridges around the Kharod estuary can be interpreted as a gradual recession of the sea (see Fig. 3A).

Site-1b (Kharod River section, 22.857521°N, 69.228848°E)

The well-sorted, medium-fine sand in the lowermost unit-I suggests deposition proximal to the trunk channel by a low-energy meandering fluvial system (Goudie, 1983; Willis

Table 5. The radiocarbon ages obtained on samples collected from India Bridge and Nani Cher. The reservoir correction age ($\Delta R \pm \sigma$) was 135 ± 86 years (Bhushan et al., 1994; Dutta et al., 2001).

Samples	Radiocarbon age in years	Calibrated age at 1σ	Average age
IB-shell	1603 ± 145	cal BP 870: cal BP 1216	1045 ± 175
Kld-shell	3498 ± 87	cal BP 3056: cal BP 3366	3210 ± 155

Notes: IB = India Bridge, Kld = Kali Nadi

and Behrensmeier, 1994). The overlying and laterally persistent bedded calcrete (unit-II) indicates the upward migration of carbonate-rich subsurface water along the riverbanks (the channel proximal to the riverine playa environment) during periods of prolonged dryness (Goudie, 1983). Such a geomorphic setting, coupled with dry climatic conditions, favored the development of bedded calcretes due to the evaporation-controlled fluctuations in the ground water (McCarthy and Metcalfe, 1990).

The cross- and trough-stratified rolled calcrete-dominated horizon (unit-III) and the crudely stratified rounded to sub-rounded calcrete gravels (unit-IV) suggest episodic mobilization of unconsolidated bed material during the occasional intense rainfall events (Reid and Frostick, 1997). Dominance of rolled calcrete implies a poorly vegetated river catchment that facilitated the erosion of pre-existing alluvial carbonates by frequent channel migration (bank undercutting and collapse). The decreasing amplitude of trough cross beds in the upper part suggests declining flow through time (Miall, 1977; Juyal et al., 2000). The large variability in the grain size in units-III and -IV (sand to gravel) could be due to the high bed load transport rates and infrequent short-lived floods (Nanson and Tooth, 1999; Tooth, 2000).

The uppermost massive, fractured dark brown sandy-clay (unit-V) indicates deposition dominantly under suspension that falls out away from the tidal channel in the middle tidal regime (Dalrymple et al., 2012; Rick et al., 2017). The low C/N ratio (<10) (see Fig. 5C) implies that the organic matter and the nitrogen were largely contributed from the marine source (Bordovskiy, 1965; Prah et al., 1980). The presence of *Rhizophora mucronata* in the lower part of unit-V suggests that the site was inundated by tidal flooding, whereas the appearance of *Avicennia marina* in the upper part points toward the declining tidal influence (Banerji et al., 2015). The intertidal deposits are located ~ 1 km inland, indicating frequent tidal inundation with a decrease in the tidal influence and suggesting gradual change toward the middle intertidal zone.

Site-2 (India Bridge section, 23.977750°N, 69.757433°E)

Texturally, gray sticky tidal clay (unit-I) with intact gastropod shells (*Melania striatella tuberculata*) suggests low-energy conditions, which facilitated the deposition of clay as a

suspension fall out (Christiansen et al., 2006) in a distal/upper tidal-flat environment (Tyagi et al., 2012). The overlying, clayey-sand (unit-II) suggests gradual withdrawal of the distal tidal-flat sedimentation and contribution of aeolian sand from the proximal areas. Both unit-I and unit-II have relatively high C_{org} and N_{total} , and the C/N is <10 , thus suggesting deposition under an intertidal environment. The overlying less fine to very fine, moderately well-sorted sand units (III and IV) (see Supplementary Table S1) indicate deposition as a source proximal obstacle aeolian sand sheet (see Fig. 6).

Site-3 (Nani Cher Archaeological mound, 23.795944°N, 68.678600°E)

The dominance of coarse pebbly sand at the lowermost unit-I suggests mobilization of coarse detritus from the surrounding upland (via fluvial channel activity) during the low stand. The bottom of this unit extends below the modern tidal flat, further suggesting that deposition occurred during lower sea level compared to the present. The overlying archaeological deposit (unit-II) indicates human occupation. The topmost rubified aeolian sand (unit-III) can be interpreted as deposition under drier conditions.

Sediment provenance

The trace element plots (see Fig. 8) show that the trend for Site-1a (estuary, unit-III), Site-1b (river section, unit-V), and the modern intertidal clay closely follow the Indus delta sediments trend. The Indus delta sediments are thought to have been routed by the alongshore current toward the Gulf of Kachchh (Ramaswamy et al., 2007; Ferrier et al., 2015). Similarly, unit-II of Site-1a also follows the Indus delta trend because there is a significant contribution of the translocated clay from the overlying unit-III. However, as can be seen, the Indus delta sediments have high elemental concentrations, which can be attributed to the size-sorting effect (McLennan, 1993), whereas the enriched Sr in modern sediments can be attributed to the greater influence of seawater. The contribution from the primary rock basalt in the river catchment can also be observed in the REEs from Nd to Lu. The mixing of the source sediment seems reasonable in intertidal deposits as sediment is derived from both the continent and sea. The trend of sandstone is not plotted given the low concentration of REE and its derivation from the primary igneous rock basalt.

Estimation of RSL

Sedimentology, geochemistry, trace fossils, C/N ratios, and palynological evidence are used to demonstrate that the clayey deposits (unit-III at Site-1a [Kharod Estuary], unit-V at Site-1b [Kharod River section], and units-I and -II at INB [Site-2]), were deposited under intertidal environments (discussed above), and are used to estimate the RSL changes.

At the Kharod Estuary (Site-1a), the top of the lower intertidal deposits (unit-III, 4.7 ± 0.2 ka) is taken as the marine

limiting data point and the bottom (7.3 ± 0.4 ka) is taken as the SLIP at 2.38 m amsl (Es). The beach ridge (unit-IV, 4.3 ± 0.2 ka) and the fluvial deposits (unit-II, 9.9 ± 0.7 , 9.3 ± 0.4 ka) are used as terrestrial limiting data points during low stand. The modern analog of lower intertidal flat deposits is exposed during low tide and inundated in high tide. The average surface elevation of the mudflats (0.96 m) lies between MLWS and MLWN (see Table 1 and Supplementary Tables S3 and S4). The RSL is calculated as 1.42 ± 0.38 m amsl (see Table 1 and Supplementary Table S1). The supporting evidence of low stand at 2.9 ± 0.2 ka and 3210 ± 155 cal yr BP is obtained from the Nani Cher section (Site-3), where the bottom fluvial unit-I extends below the modern tidal flat as the modern tidal flat abuts it (see Fig. 7).

At the Kharod River section (Site-1b), the middle-low intertidal deposits (unit-V; 6.8 ± 0.5 ka) are taken as SLIP at 4.6 m amsl (Es). The terrestrial limiting data point is not marked as the transition from fluvial, and the tidal sequence is not dated. The modern analog (mudflat) laterally abuts the studied section and is exposed during low tide, where the average surface elevation of mudflats (1.3 m) lies between MLWN and MHWN (see Table 1 and Supplementary Tables S3 and S4). The RSL is calculated as 3.3 ± 0.53 m amsl.

The Rann surface elevation around INB (Site-2) is ~ 3.6 m above the present sea level (see Fig. 2), and the locality is inundated only by the Indian Summer Monsoon (ISM) wind-induced tidal surges (Roy and Merh, 1982; Tyagi et al., 2012). The upper part of unit-II (intertidal deposits) represents a transitional phase, and the contact with unit-III is not sharp. The dominance of upper intertidal sedimentation is inferred based on a relatively high concentration of clay facies and an increase in C/N ratio, which is at 2.8 m amsl (Es) (see Fig. 6). This is used as SLIP for the Late Holocene (1045 ± 175 cal yr BP, 1.1 ± 0.1 ka). The terrestrial limiting data point is ascertained based on beach ridge deposits (unit-III, 0.8 ± 0.04 ka). Due to the concealment of the base of unit-I, the marine limiting data point is not marked. The modern analog is located at Sunda high, which is exposed during low tide, with an average surface elevation of mudflats (2.1 m) close to the MHWN recorded at distal Okha station (see Table 1 and Supplementary Table S4), ~ 100 km south of INB section. The RSL is calculated as 0.73 ± 0.43 m amsl.

One of the major factors affecting the RSL change estimation is the sediment compaction. Since the intertidal facies are low in organic component and contain sand facies, the compaction of the sediments can be treated as minimal (Brain et al., 2012; Hijma et al., 2015). However, the estimates are subjected to tectonic correction (see Table 1).

Tectonic correction

Various uplift rate estimates exist from the region ranging from 0.3 mm per year to as high as 4 mm per year (Bhattacharya et al., 2014; Kothiyari et al., 2016; Prizomwala et al., 2016). These estimates are largely obtained using one location age-depth relationship of the bedrock strath surface and

do not account for the two-dimensional geometry of the strath surface elevation as a function of river gradient. For realistic uplift rate estimates, the age and height of the strath above the riverbed should be measured along the river at multiple locations. The regression slope of the plot of incision depth versus the ages obtained at multiple locations will give the time average incision rate (Wegmann and Pazzaglia, 2009; Bhattacharya et al., 2019). Thus, in the present study, we have used the estimates from Bhattacharya et al. (2019). They suggested the uplift rate for the Wagad upland located in the northeast of Site-1 as 0.06 ± 0.01 mm/yr, and for Pachcham Island located in the proximity of Site-2 as 0.2 ± 0.01 mm/yr. We used the average of these estimates (0.13 ± 0.01 mm/yr) for the Kharod estuary and river sections (Site-1a and Site-1b), whereas for the INB section (Site-2), the uplift rate of Pachcham Island is used (see Table 1). Detailed calculations of SLIP, RWL, Es, IR, and RSL and an estimation of the tectonic component are given in the supplementary data (see Supplementary Tables S1–S3). Thus, at Site-1a and Site-1b, the average RSL change after accounting for the tectonic component is 1.45 ± 0.33 m amsl, and at Site-2 it is 0.53 ± 0.43 m amsl (Fig. 9, see Table 1).

Changes in land-sea configuration

The sedimentological evidence along with the optical chronology suggests that prior to ~ 9 ka, the fluvial system prograded toward the exposed shelf of the Gulf of Kachchh. This is in conformity with the observation made by Vora et al. (1996) that the pre-Holocene shoreline along the coast of India is represented by the shelf edge reefs, occurring at water depths from -136 to -85 m. Furthermore, the occurrence of dolomite crust at a depth of -35 m dated to ~ 14 ka (Rao et al., 2003) suggests that sea level was lower by at least 35 m. Similar inferences are drawn based on the seismic sequence stratigraphy data from the Gulf of Kachchh by Michael et al. (2009). The presence of channel gravel overlain by the sandy horizons of units-I and -II at the Kharod Estuary (Site-1a) and units-I to -IV at the Kharod River section (Site-1b) (see Figs. 4 and 5) suggest frequent shifting of the river course. As a consequence, the deposits are an amalgamation of individual channel-belt gravels overlain by sandy fluvial deposits (Jensen and Pedersen, 2010). Additionally, a large part of the continental shelf is exposed to rainfall runoff, which leads to the development of incised valleys and an associated fluvial channel network (Fagherazzi et al., 2004) as observed in the coast-proximal region of the Kharod River. Compilation of the late Pleistocene–Holocene sea-level data from the western continental margin by Hashimi et al. (1995) indicates a sharp rise in sea level after 9 ka, although sea level was still lower than the present by ~ 20 m. Our data indicate RSL of 1.45 ± 0.33 m at ~ 7 ka and transition toward a tidal environment with deposition by hydrodynamic processes of waves and tides along the coast and estuaries (Orton and Reading, 1993) that continued until ~ 5 ka. Thus, the period is interpreted as a stable high stand having positive tendency as the marine influence

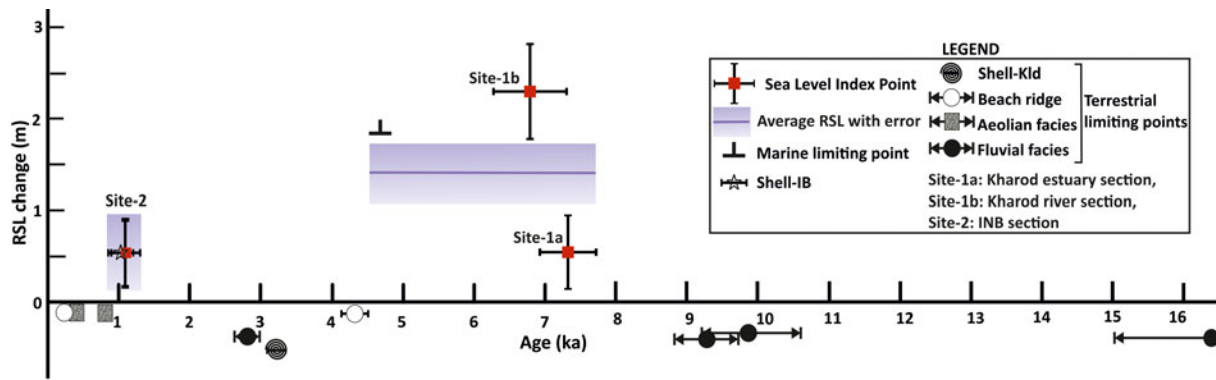


Figure 9. Age-elevation plot of the mid and late sea-level index points (SLIPs) and terrestrial and marine limiting points. The associated errors in RSL and chronology are shown by vertical and horizontal bars, respectively. The Mid-Holocene RSL (~7–5 ka) (blue stippling) is the average of RSL based on SLIPs at Sites-1a and -1b. Based on terrestrial limiting data points, we suggest that the negative tendency might have begun ~4.5 ka. The Late Holocene RSL (~1 ka) (blue stippling) is marked from SLIP at Site-2. (For interpretation of the references to color in this figure legend, the reader is referred to the web version of this article.)

increased steadily (see Fig. 9) while the ISM declined (Schulz et al., 1998; Bhushan et al., 2018). The overlying older beach ridge (unit-IV) dated to ~4 ka (see Fig. 4) suggests gradual regression of the sea toward its present position following the regional aridity (4.2 ka event). Around 1 ka, at INB (Site-2), RSL of 0.53 ± 0.43 m amsl could have been due to the surface inundation by monsoon wind-driven tide surges as the tidal amplitude changed during the marginal high stand. At present, an analogous situation prevails ~50 km south of the INB toward Kori Creek near Sunda High (Merh, 2005). The event was not observed at Site-1a and -1b. We suggest that even if the deposition occurred in the Kharod Estuary, it would have been in a channel-proximal location and farther toward the sea (due to its lower magnitude), and therefore subsequently eroded by wave action as compared to Site-2 which is more distal and sheltered. The sea seems to have regressed in phases thereafter as indicated by obstacle dune sheet deposits at Site-2 (unit-III) dated to ~0.8 ka (see Fig. 6) and the reworked aeolian sand (unit-V) dated to ~0.4 ka (unit-IV, Site-1a) (see Fig. 4). The sea level largely stabilized during the last 0.2 ka (end of Little Ice Age) as suggested by the age of the younger (modern) beach ridge at the Kharod Estuary (Site-1a, see Fig. 3).

Thus, summarizing the observations presented above, it can be suggested that the Gulf of Kachchh experienced two events of high stand during the Mid- to Late Holocene. The tectonically corrected Mid-Holocene high stand was below ~1.5 m, whereas the Late Holocene high stand was only marginally higher (see Fig. 9).

Causes of Holocene RSL changes

In far-field locations from ice sheets, the eustatic component (glacial melt and hence the climate) can only be ascertained if the non-eustatic components are reasonably accounted for (Mitrovica and Peltier, 1991). The Gulf of Kachchh can be compared with the farthest location in Zone III (Clark et al.,

1978) with minimal glacial and hydro-isostatic components (Fleming et al., 1998; Mitrovica and Milne, 2002). However, the Gulf of Kachchh has relatively shallow continental shelf depth, which varies from 50 to 130 m (Chauhan and Almeida, 1993). Therefore, the Mid-Holocene RSL change of 1.45 ± 0.33 m may be affected by GIA (the response of solid earth to redistribution of both ice and water [continental levering]) along with land elevation changes due to tectonics (already considered); high sedimentation rates from the Indus delta (Mitrovica and Milne, 2002; Ferrier et al., 2015); and the meltwater flux from the northern ice sheets and the Himalayan cryosphere.

In the far-field continental margin regions like the Gulf of Kachchh, the effect of ice-isostasy is overwhelmed by continental levering (hydro-isostasy): coastlines and continental interiors are uplifted due to water loading of the continental shelf to produce local sea-level falls that are surrounded by offshore bands experiencing sea-level rise (Mitrovica and Milne, 2002; Lambeck et al., 2010, 2014). However, the deposition of sediment in a source-proximal coastal region like the Indus delta is thought to cause crustal subsidence and induce rise in sea level (Ferrier et al., 2015). This effect partially counterbalances the fall in sea level due to ocean siphoning and continental levering (Dalca et al., 2013; Whitehouse, 2018). The Indus River is the fifth-largest contributor of sediment to the world oceans (Wells and Coleman, 1984) as it drains high relief and barren landscape containing large volumes of (para) glacial debris in its upper reaches (Milliman et al., 1984); therefore, it can produce meter-scale changes in sea level near the delta (Ferrier et al., 2015). Geomorphological studies suggest that the Indus delta (see Fig. 1) was more proximal to the study area during the Mid-Holocene (Snelgrove, 1979; Flam, 1993) and also contributed enhanced sedimentation, particularly after 7 ka due to the reworking of terrace deposits and the sediment of lower alluvial plains (Clift et al., 2012; Clift and Giosan, 2014). If the global average of hydrostatic sea-level fall (0.2–0.4 mm/yr) during the

Holocene (Lambeck et al., 2010) is considered, it would result in 0.5–0.8 m of sea-level fall at the site between ~7 and 5 ka. A regional model, after accounting for both the GIA and sediment deposition, estimated RSL change at Karachi and Saurashtra as –1 and +0.5 m, respectively, during 7–5 ka (Ferrier et al., 2015). Since the present study is located in the vicinity of Karachi and Saurashtra, we argue that the area receives only marginal contribution from GIA and sediment bulking in the RSL estimate of 1.45 ± 0.33 m (tectonically corrected).

The drowned coral reefs and the sedimentary sequences from deltas and estuaries suggest that meltwater pulses from the large Northern Hemisphere, as well as Antarctic ice sheets, had largely ceased by ~7 ka (Blanchon and Shaw, 1995; Lambeck, et al., 2002; Hori and Saito 2007; Harris et al., 2008). However, studies suggest that during the Mid-Holocene, a phase of deglaciation was witnessed in the upper Indus River basin (Sharma et al., 2016; Ganju et al., 2018; Sharma and Shukla, 2018), which added a meltwater pulse from the Himalayan cryosphere. Therefore, we suggest that the observed RSL high stand during the Mid-Holocene has a large contribution from the increased glacial melt from the upper Indus basin in addition to the marginal contribution from the northern ice sheets during the Mid-Holocene. The effect of GIA probably dominated only once the eustatic changes resulting from meltwater were minimal (Milne et al., 2005), and therefore induced sea-level fall.

The Late Holocene RSL change of 0.53 ± 0.43 m dated to ~1 ka corresponds to the Medieval Warm Phase (MWP) (Lamb, 1965). Studies indicate that the MWP was a phase of strengthened ISM. For example, the geochemical evidence from the ISM-dominated central Himalayan lake record indicates increased flux of the detrital proxies (Bhushan et al., 2018). The fluvial system in southern (Thomas et al., 2007), central (Kale et al., 2003), and western India (Kale et al., 2000; Bhattacharya et al., 2014) recorded regional floodplain aggradation during the MWP. Globally, the MWP is not associated with significant sea-level oscillations (Lambeck et al., 2014), which are suggested to have been no more than 0.1 ± 0.1 mm/y until ~1.3 ka; after 1 ka the fall in sea level is ascribed to the global cooling of 0.2°C (Kopp et al., 2016). In the eastern Arabian Sea, the temperature and glacial meltwater changes are thought to have been negligible during the last 3 ka (Chauhan et al., 2010); hence, it seems unlikely that steric changes caused the RSL high. Changes in the tidal amplitudes in the delta settings are also suggested as a cause of minor RSL changes (van de Plassche et al., 1998). Since the low-lying Great Rann is frequently inundated by the monsoon wind-induced tidal surges in summer (Glennie and Evans, 1976), we hypothesize that during the MWP, increased ISM strength (Chauhan et al., 2010) would have significantly amplified the wind-induced tidal ingress to cause tidal amplitude changes that led to the deposition of the tidal clay in the distal low-lying area of Kori Creek (see Fig. 1).

Implication for the coastal Harappan settlements

The material culture of Harappans suggests their contact with contemporaneous Mesopotamia and Egyptian civilizations, and the importance of sea trade routes for Harappan commerce is reasonably well established (Khan, 1955). For example, the discovery of Indus-type stamp seals in southern Mesopotamia and the Persian Gulf area suggested that a part of the Mesopotamia seafaring activities was directed toward the east (Dales, 1962). Early explorations (Stein, 1931; Dales, 1962) identified Harappan outposts along the Makran coast, suggesting the prevalence of sea trade. Similarly, out of 19 Harappan sites reported from the Kachchh region, nine are from the Great and Little Rann and the remaining are located along the coastal region of the Gulf of Kachchh (see Fig. 1B), suggesting a preference for proximity to the sea (Rawat, 2015). The majority of the sites dated belong to the Mature Harappan period (4600–3900 yr BP); the two exceptions are from the Late Harappan period (3900–3300 yr BP) (Kenoyer, 1998; Wright et al., 2008; Rawat, 2015).

The previous estimates of RSL changes (Gaur and Vora, 1999; Gaur et al., 2013; Das et al., 2017; Makwana et al., 2019) suggested that the withdrawal of the Mid-Holocene high stand was critical to the abandonment/desertion of the coastal Harappan settlements (Saurashtra and Kachchh). The RSL estimates obtained in these studies were not based on the standardized protocol such as the SLIPs, RWL, IRs, etc. Therefore, confidence in the RSL estimate remains low; thus, their suggestion about the deterministic role of sea-level changes and emergence and desertion of Harappan settlements remains speculative. For example, Gaur et al. (2013) suggested the higher RSL at ~6 ka, which is inferred from Barbados (Fairbanks, 1989). Das et al. (2017), suggested an ~2-m-high sea level during 6–3 ka from the Kharod Estuary (Site-1a of the present study) where fine sand and silty-sand (units-3–6) were ascribed to estuarine/beach face environments and the high sea level was estimated from 10-cm-thick marine shell-rich horizon (unit-5). We could not verify the diagnostic marine shell layer of Das et al. (2017) during our field survey (see Fig. 4). Therefore, the RSL estimate and inference based on it about the role of high sea level in the abandonment of Harappan settlements remains inconclusive. More recently, Makwana et al. (2019) estimated a 2-m high stand at ~2.9 ka from the Banni plain flanking the eastern margin of Kori Creek (Kachchh) and correlated it with the port settlements of the Late Harappan period. The 2.9 ka age is obtained from a clay unit located at a depth ~4 m below the surface, which is 2 m above the present sea level (Makwana et al., 2019). This would mean that at ~2.9 ka, the sea was –2 m below the present sea level and not +2 m (see fig. 3 of Makwana et al., 2019). Furthermore, the chronology does not conform to the Mid-Holocene or the Harappan period but corresponds to the early Iron Age culture in the Late Holocene (Sarkar et al., 2020).

The present study, therefore, becomes important as it fills this gap; the tectonically corrected high RSL of

1.45 ± 0.33 m between ~7 and 5 ka is estimated following the standard protocol, which predates the early Mature Harappan period (4.6–3.9 ka) (Kenoyer, 1998; Wright et al., 2008; Sarkar et al., 2016). We hypothesize that the sea occupied the creeks and estuaries and intertidal swampy pools in the Rann during high stand (~7–5 ka) and provided a favorable environment for the growth of mangroves and an additional source of seafood (Lawler, 2011; Sengupta et al., 2020). As the sea regressed, it could only have shrunken the channel width of the creeks (van de Plassche et al., 1998). The elevations of some of the important archaeological sites (e.g., Juni Kuran, 3.6 m; Dholavira, 2.03 m; Kanmer, 3.63 m; and Bagasara, 4.3 m) (see Fig. 1B) further indicate that sea was at a distance from these locations, and most likely accessible through creeks. It was certainly not close to the Harappan settlements as is also indicated by the deposition of fluvial sediments near the Khadir Island (Dholavira) during the Harappan time (Ngangom et al., 2016). Additionally, *Turbinella Pyrum* (conch shell) collected ~60 cm above the high tide mark at Nani Cher archaeological mound (near Lakhpat) is radiocarbon dated to 3200 cal yr BP; the sediment is dated to 2.9 ± 0.2 ka (see Fig. 7). This further indicates that the sea level was significantly lower during the latter part of the Mid-Holocene, which also accords well with Tyagi et al. (2012). Therefore, it seems more plausible to suggest that (i) the Mid-Holocene RSL high had no defining role in the urbanization or evolution of the coastal Harappan settlements, and (ii) the sea-level influence seems to have been limited because the intertidal environment could have provided the optimal environment for additional food resources.

CONCLUSIONS

The relict intertidal deposits from the Kharod River Estuary, Gulf of Kachchh, and the distal end of Kori Creek are used to infer the Mid- to Late Holocene RSL. Based on sedimentology, geochemistry, palynology, ichnology, and optical and radiocarbon dating, the study suggests that fluvial activity dominated between 16.5 ± 1.6 and 9.9 ± 0.7 ka. During this period, sea level was significantly lower than the present, and ephemeral streams extended their course into the shallow shelf of the Gulf of Kachchh. After ~7 ka the sea level showed a positive tendency until ~5 ka. The tectonically corrected Mid-Holocene RSL, based on the estimates from the northern and eastern part of the Kachchh Peninsula, is 1.45 ± 0.33 m and is estimated by comparing the relict intertidal deposits with modern analogs. The study suggests that the Mid-Holocene RSL in the Gulf of Kachchh was largely due to the meltwater contribution from the Himalayan cryosphere, while GIA and crustal subsidence due to sediment bulking supplemented it. The Late Holocene (1.1 ± 0.1 ka and 1045 ± 175 cal yr BP) tectonically corrected RSL change is estimated as 0.53 ± 0.43 m and corresponds to the MWP. We attribute the marginal RSL high to monsoon wind-driven tidal ingression that might have affected the tidal amplitude positively. Furthermore, our study suggests that the Harappan settlements along the coast flourished during the recessional

phase of the Mid-Holocene high sea level. This would imply that there was no deterministic role of the Mid-Holocene high sea level in the evolution and abandonment of the Harappan settlements. Instead, the sea-level influence seems to have been limited because the intertidal environment could have provided additional food resources for their sustenance.

ACKNOWLEDGMENTS

Authors are thankful to the editors and four anonymous reviewers for their comments and valuable suggestions. We are thankful to Dr. M.G. Yadava who provided the radiocarbon ages. Prof. M.G. Thakkar, Dr. Naveen Chauhan, and the students of the K.S.K.V. Kachchh University—Anil Chavan, Ketan Chaskar, and Jangir Jagdish—are acknowledged for their valuable help during the fieldwork. The proprietor of KARM construction, Bhuj, is thanked for the DGPS instrument. Navin Juyal expresses profound gratitude toward Gurudev (Dr. R. K. Pant) for his guidance. Shilpa Pandey is thankful to the Director, BSIP, for permission to carry out palynological studies.

SUPPLEMENTARY MATERIAL

The supplementary material for this article can be found at <https://doi.org/10.1017/qua.2020.86>

REFERENCES

- Aitken, M.J., 1998. *Introduction to optical dating: the dating of Quaternary sediments by the use of photon-stimulated luminescence*. Clarendon Press, New York.
- Ajithprasad, P., 2006. The Harappan Black Slipped Jar from Bagasara, Gujarat and its Significance. Pre-print of paper presented in the International Seminar on Magan and Indus Civilization, organized by ASI and M S University of Baroda.
- Allen, J.R.L., Angela, L.L., Drak, P., 2007. Seasonality of $\delta^{13}\text{C}$ and C/N ratios in modern and mid-Holocene sediments in the Severn Estuary levels, SW Britain. *The Holocene* 17, 139–144.
- Bailey, R.M., Arnold, L.J., 2006. Statistical modelling of single grain quartz De distributions and an assessment of procedures for estimating burial dose. *Quaternary Science Review* 25 (19–20), 2475–2502.
- Banerjee, D., Murray, A.S., Bøtter-Jensen, L., Lang, A., 2001. Equivalent dose estimation using a single aliquot of polymineral fine grains. *Radiation Measurements* 33, 73–94.
- Banerjee, P.K., 1993. Imprints of late Quaternary climatic and sea level changes on East and South Indian coast. *Geo-Marine Letters* 13, 56–60.
- Banerjee, P.K., 2000. Holocene and Late Pleistocene relative sea level fluctuations along the east coast of India. *Marine Geology* 167, 243–260.
- Banerji, U.S., Pandey, S., Bhushan, R., Juyal, N., 2015. Mid-Holocene climate and land–sea interaction along the southern coast of Saurashtra, western India. *Journal of Asian Earth Sciences* 111, 428–439.
- Bezerra, F.H.R., Vita-Finzi, C., Lima Filho, F.P., 2000. The use of marine shells for radiocarbon dating of coastal deposits. *Revista Brasileira de Geociências* 30, 211–213.

- Bhattacharya, F., Chauhan, G., Prasad, A.D., Patel, R.C., Thakkar, M.G., 2019. Strike-slip faults in an intraplate setting and their significance for landform evolution in the Kachchh peninsula, Western India. *Geomorphology* 328, 118–137.
- Bhattacharya, F., Rastogi, B.K., Thakkar, M.G., Patel, R.C., Juyal, N., 2014. Fluvial landforms and their implication towards understanding the past climate and seismicity in the northern Katrol Hill Range, western, India. *Quaternary International* 333, 49–61.
- Bhatt, N., Bhande, U., 2006. Geomorphologic expression of late Quaternary sea level changes along the southern Saurashtra coast, western India. *Journal of Earth System Science* 115, 395–402.
- Bhushan, R., Chakraborty, S. and Krishnaswami, S., 1994. Physical research laboratory (chemistry) radiocarbon date list I. *Radiocarbon* 36, 251–256.
- Bhushan, R., Sati, S.P., Rana, N., Shukla, A.D., Mazumdar, A.S., Juyal, N., 2018. High-resolution millennial and centennial scale Holocene monsoon variability in the Higher Central Himalayas. *Palaeogeography, Palaeoclimatology, Palaeoecology* 489, 95–104.
- Biswas, S.K., 2016. Tectonic Framework, Structure and Tectonic Evolution of Kutch Basin, Western India. In Conference GSI, 129–50. DOI: 10.17491/cgsi/2016/105417
- Blanchon, P., Shaw, J., 1995. Reef drowning during the last deglaciation: evidence for catastrophic sea-level rise and ice-sheet collapse. *Geology* 23, 4–8.
- Bordovskiy, O.K., 1965. Accumulation and transformation of organic substances in marine sediments. *Marine Geology* 3, 5–31.
- Bøtter-Jensen, L., Thomsen, K.J., Jain, M., 2010. Review of optically stimulated luminescence (OSL) instrumental developments for retrospective dosimetry. *Radiation Measurements* 45, 253–257.
- Brain, M.J., Long, A.J., Woodroffe, S.A., Petley, D.N., Milledge, D.G., Parnell, A.C., 2012. Modelling the effects of sediment compaction on salt marsh reconstructions of recent sea-level rise. *Earth and Planetary Science Letters* 345, 180–193.
- Brückner, H., 1989. Late Quaternary shorelines in India; In: Scott, D.B., Pirazoli, P.A., Honig, C.A., (Eds.), *Late Quaternary sea-level correlation and applications*. Kluwer Academic Publisher, pp. 169–194.
- Buatois, L.A., Mángano, M.G., 2011. *Ichnology: Organism-Substrate interaction in space and Time*. Cambridge University Press, New York, p. 1–358.
- Burow, C., 2019. calc_CentralDose: Apply the central age model (CAM) after Galbraith et al. (1999) to a given De distribution. version 1.4.0. 2019 In: Kreuzer, S., Burow, C., Dietze, M., Fuchs, M.C., Schmidt, C., Fischer, M., Friedrich, J. (Eds.), *Luminescence: Comprehensive Luminescence Dating Data Analysis*. R Package Version 0.9.5, <https://CRAN.R-project.org/package=Luminescence>.
- Chauhan, O.S., Almeida, F., 1993. Influences of Holocene sea level, regional tectonics, and fluvial, gravity and slope currents induced sedimentation on the regional geomorphology of the continental slope off northwestern India. *Marine Geology* 112, 313–328.
- Chauhan, O.S., Vogelsang, E., Basavaiah, N., Kader, U.S.A., 2010. Reconstruction of the variability of the southwest monsoon during the past 3 ka, from the continental margin of the southeastern Arabian Sea. *Journal of Quaternary Science* 25, 798–807.
- Christiansen, C., Vølund, G., Lund-Hansen, L.C., Bartholdy, J., 2006. Wind influence on tidal flat sediment dynamics: Field investigations in the Ho Bugt, Danish Wadden Sea. *Marine Geology* 235, 75–86.
- Clark, J.A., Farrell, W.E., Peltier, W.R., 1978. Global changes in postglacial sea level: a numerical calculation. *Quaternary Research* 9, 265–287.
- Clift, P.D., Carter, A., Giosan, L., Durcan, J., Duller, G.A.T., Macklin, Mark G., Alizai, A., et al., 2012. U-Pb zircon dating evidence for a Pleistocene Sarasvati River and capture of the Yamuna River. *Geology* 40, 211–214.
- Clift, P.D., Giosan, L., 2014. Sediment fluxes and buffering in the post-glacial Indus Basin. *Basin Research* 26, 369–386.
- Clift, P.D., Giosan, L., Carter, A., Garzanti, E., Galy, V., Tabrez, A.R., Pringle, M., et al., 2010. Monsoon control over erosion patterns in the western Himalaya: possible feed-back into the tectonic evolution. *Geological Society, London, Special Publications* 342, 185–218.
- Compton, J.S., Franceschini, G., 2005. Holocene geoarchaeology of the Sixteen Mile Beach barrier dunes in the Western Cape, South Africa. *Quaternary Research* 63, 99–107.
- Daidu, F., Yuan, W., Min, L., 2013. Classifications, sedimentary features and facies associations of tidal flats. *Journal of Palaeogeography* 2, 66–80.
- Dalca, A.V., Ferrier, K.L., Mitrovica, J.X., Perron, J.T., Milne, G.A., Creveling, J.R., 2013. On postglacial sea level—III. Incorporating sediment redistribution. *Geophysical Journal International* 194, 45–60.
- Dales, G.F., 1962. Harappan outposts on the Makran coast. *Antiquity* 36, 86–92.
- Dalrymple, R.W., Mackay, D.A., Ichaso, A.A., Choi, K.S., 2012. Processes, morphodynamics, and facies of tide-dominated estuaries. In: Davis Jr. R., Dalrymple R. (eds) *Principles of Tidal Sedimentology*. Springer, Dordrecht, pp. 79–107 https://doi.org/10.1007/978-94-007-0123-6_5.
- Das, A., Prizomwala, S.P., Makwana, N., Thakkar, M.G., 2017. Late Pleistocene-Holocene climate and sea level changes inferred based on the tidal terrace sequence, Kachchh, Western India. *Palaeogeography, Palaeoclimatology, Palaeoecology* 473, 82–93.
- Day, J.W., Gunn, J.D., Folan, W.J., Yanez-Arancibia, A., Horton, B.P., 2007. Post-glacial coastal margin productivity and the emergence of civilizations. *Eos Transactions AGU* 80, 170–171.
- Desai, B.G., 2016. Ichnological analysis of the Pleistocene Dwarka Formation, Gulf of Kachchh: trace maker behaviors and reworked traces. *Geodinamica Acta* 28, 18–33.
- Desai, B.G., Patel, S.J., 2008. Trace Fossil Assemblages (Ichnocoenoses) of the Tectonically Uplifted Holocene Shorelines, Kachchh, Western India. *Journal of the Geological Society of India* 71, 527–540.
- Desjardins, P.R., Buatois, L.A., Mángano, M.G., 2012. Tidal flats and subtidal sand bodies. In: Dirk Knaust, Richard G. Bromley (eds) *Developments in Sedimentology* 64, 529–561. Elsevier.
- Dunn, R.J., Welsh, D.T., Teasdale, P.R., Lee, S.Y., Lemckert, C.J., Méziane, T., 2008. Investigating the distribution and sources of organic matter in surface sediment of Coombabah Lake (Australia) using elemental, isotopic and fatty acid biomarkers. *Continental Shelf Research* 28, 2535–2549.
- Durcan, J.A., King, G.E., Duller, G.A., 2015. DRAC: Dose Rate and Age Calculator for trapped charge dating. *Quaternary Geochronology* 28, 54–61.
- Dutta, K., Bhushan, R., Somayajulu, B., 2001. ΔR correction values for the northern Indian Ocean. *Radiocarbon* 43, 483–488. Encyclopedia of Earth Science Series. Springer, Dordrecht.

- Engelhart, S.E., Vacchi, M., Horton, B.P., Nelson, A.R., Kopp, R.E., 2015. A sea-level database for the Pacific coast of central North America. *Quaternary Science Reviews* 113, 78–92.
- Erdtman, G., 1943. *An introduction to pollen analysis*. Chronica Botanica, Waltham Massachusetts.
- Fagherazzi, S., Howard, A.D., Wiberg, P.L., 2004. Modeling fluvial erosion and deposition on continental shelves during sea level cycles. *Journal of Geophysical Research* 109 (F3), F03010, 10.1029/2003JF000091.
- Fairbanks, R.G., 1989. A 17,000-year glacio-eustatic sea level record: influence of glacial melting rates on the Younger Dryas event and deep-ocean circulation. *Nature*, 342, 637–642.
- Ferrier, K. L., Mitrovica, J.X., Giosan, L., Clift, P.D., 2015. Sea-level responses to erosion and deposition of sediment in the Indus River basin and the Arabian Sea. *Earth and Planetary Sciences Letters* 416, 12–20.
- Flam, L., 1993. Fluvial geomorphology of the lower Indus basin (Sindh, Pakistan) and the Indus civilization. J.F. Shroder (Ed.), *Himalaya to the sea*. Routledge, London, pp. 265–287.
- Fleming, K., Johnston, P., Zwart, D., Yokoyama, Y., Lambeck, K., Chappell, J., 1998. Refining the eustatic sea-level curve since the Last Glacial Maximum using far-and intermediate-field sites. *Earth and Planetary Science Letters* 163, 327–342.
- Fuchs, M.C., Gloaguen, R., Krbetschek, M., Szulc, A., 2014. Rates of river incision across the main tectonic units of the Pamir identified using optically stimulated luminescence dating of fluvial terraces. *Geomorphology* 216, 79–92.
- Galbraith, R.F., Roberts, R.G., 2012. Statistical aspects of equivalent dose and error calculation and display in OSL dating: An overview and some recommendations. *Quaternary Geochronology* 11, 1–27.
- Ganju, A., Nagara, Y.C., Sharma, L.N., Sharma, S., Juyal, N., 2018. Luminescence chronology and climatic implication of glaciation in the Nubra valley, Karakoram Himalaya, *Palaeogeography, Palaeoclimatology, Palaeoecology*, <https://doi.org/10.1016/j.palaeo.2018.04.022>.
- Gaur, A.S., Vora, K.H., 1999. Ancient shoreline of Gujarat, India during the Indus civilization (late mid-Holocene): A case study based on archaeological evidences. *Current Science* 77, 180–185.
- Gaur, A.S., Vora, K.H., Sundaresh, R., Murali, M., Jayakumar, S., 2013. Was the Rann of Kachchh navigable during the Harappan times (Mid-Holocene)? An archaeological perspective. *Current Science* 105, 1485–1491.
- Glennie, K.W., Evans, G., 1976. A reconnaissance of the Recent sediments of the Ranns of Kutch, India. *Sedimentology* 23, 625–647.
- Goudie, A.S., 1983. Calcrete. In: Goudie, A.S., Pye, K. (Eds.), *Chemical Sediments and Geomorphology*. Academic Press, London, pp. 93–132.
- Gupta, S.K., 1975. Silting of the Rann of Kutch during Holocene. *Indian Journal of Earth Sciences* 2, p.201.
- Häntzschel, W., 1955. Tidal flat deposits (Wattenschlick). In: Trask, P.D. (ed.), *Recent Marine Sediments*. The Society of Economic Paleontologists and Mineralogists (SP4), pp. 195–226.
- Häntzschel, W., 1975. Trace fossils and problematic In: Teichert, C. (Ed.), *Treatise on invertebrate paleontology* (Part W, Miscellaneous. Supplement 1). Geological Society of America/University of Kansas Press, Boulder/Lawrence, pp. 1–269.
- Harris, P. T., Heap, A. D., Marshall, J. F., McCulloch, M., 2008. A new coral reef province in the Gulf of Carpentaria, Australia: colonisation, growth and submergence during the early Holocene. *Marine Geology* 251, 85–97.
- Hashimi, N.H., Nigam, R., Nair, R.R., Rajagopalan, G., 1995. Holocene sea level fluctuations on western Indian continental margin—an update. *Journal of the Geological Society of India* 46, 157–162.
- Hesp, P.A., 1984. Foredune Formation in Southeast Australia. In: Thom, B.G. (Ed.), *Coastal geomorphology in Australia*. Academic Press, Sydney, pp. 69–97.
- Hijma, M.P., Engelhart, S.E., Törnqvist, T.E., Horton, B.P., Hu, P., Hill, D.F., 2015. A protocol for a geological sea-level database. In: Shennan, I., Long, A.J., Horton, B.P. (Eds.), *Handbook of Sea-Level Research*. Wiley Blackwell, pp. 536–553.
- Hogg, A.G., Higham, T.F., Dahm, J., 1998. ¹⁴C dating of modern marine and estuarine shellfish. *Radiocarbon* 40, 975–984.
- Hori, K., Saito, Y., 2007. An early Holocene sea-level jump and delta initiation. *Geophysical Research Letters* 34, L18401, doi:10.1029/2007GL031029.
- Jensen, M.A., Pedersen, G.K., 2010. Architecture of vertically stacked fluvial deposits, Atane Formation, Cretaceous, Nuussuaq, central West Greenland. *Sedimentology* 57, 1280–1314.
- Johnson, D.W., 1919. *Shore Processes and Shoreline Development*. Hafner Publishing, New York.
- Juyal, N., Pant, R.K., Bhushan, R., Somayajulu, B.L.K., 1995. Radiometric dating of late Quaternary sea levels of the Saurashtra coast, Western India: an experiment with oyster and clam shells. *Geological Society of India Memoir* 32, 372–379.
- Juyal, N., Raj, R., Maurya, D.M., Chamyal, L.S., Singhvi, A.K., 2000. Chronology of late Pleistocene environmental changes in the lower Mahi basin, western India. *Journal of Quaternary Science* 15, 501–508.
- Kale, P., Singh, H., Perlmutter, H., 2000. Learning and protection of proprietary assets in strategic alliances: building relational capital. *Strategic Management Journal* 21, 217–237.
- Kale, V.S., Mishra, S., Baker, V.R., 2003. Sedimentary records of palaeofloods in the bedrock gorges of the Tapi and Narmada Rivers, central India. *Current Science* 84, 1072–1079.
- Kar, A., 1993. Neotectonic influences on morphological variations along the coastline of Kachchh, India. *Geomorphology* 8, 199–219.
- Kench, P.S., Smithers, S.G., Mclean, R.F., Nichol, S.L., 2009. Holocene reef growth in the Maldives: evidence of a mid-Holocene sea-level highstand in the central Indian Ocean. *Geology* 37, 455–458.
- Kennett, D.J., Kennett, J.P., Erlandson, J.M., Cannariato, K.G., 2007. Human responses to Middle Holocene climate change on California's Channel Islands. *Quaternary Science Reviews* 26, 351–367.
- Kenoyer, J. M., 1998. *Ancient Cities of the Indus Valley Civilization*. Oxford University Press, Oxford.
- Khan, F.A., 1955. *Fresh Sidelights on the Indus Valley and the Bronze Age Orient* (No. 4). Department of Archaeology, Annual Report of the Institute of Archaeology, pp. 51–68.
- Khonde, N., Maurya, D.M., Singh, A.D., Chowksey, V., Chamyal, L.S., 2011. Environmental significance of raised rann sediments along the margins of Khadir, Bhanjada and Kuar Bet islands in Great Rann of Kachchh, Western India. *Current Science* 101, 1429–1434.
- Knaust, D., 2017. *Atlas of Trace Fossils in Well Core: Appearance, Taxonomy, and Interpretation*. Springer, Norway.
- Kopp, R.E., Kemp, A.C., Bittermann, K., Horton, B.P., Donnelly, J.P., Gehrels, W.R., Hay, C.C., Mitrovica, J.X., Morrow, E.D., Rahmstorf, S., 2016. Temperature-driven global sea-level

- variability in the Common Era. *Proceedings of the National Academy of Sciences* 113, 1434–1441.
- Kothyari, G.C., Rastogi, B.K., Morthekai, P., Dumka, R.K., 2016. Landform development in a zone of active Gedi Fault, Eastern Kachchh rift basin, India. *Tectonophysics* 670, 115–126.
- Ku, H.W., Chen, Y.G., Liu, T.K., 2005. Environmental Change in the Southwestern Coastal Plain of Taiwan since Late Pleistocene: Using Multiple Proxies of Sedimentary Organic Matter. *TAO* 16, 1079–1096.
- Kunte, P.D., Wagle, B.G., 2005. The beach ridges of India: a review. *Journal of Coastal Research* 42, 174–183.
- Lambeck, K., Esat, T.M., Potter, E.K., 2002. Links between climate and sea levels for the past three million years. *Nature* 419, 199–206.
- Lambeck, K., Rouby, H., Purcell, A., Sun, Y., Sambridge, M., 2014. Sea level and global ice volumes from the Last Glacial Maximum to the Holocene. *Proceedings of the National Academy of Sciences* 111, 15296–15303.
- Lambeck, K., Woodroffe, C.D., Antonioli, F., Anzidei, M., Gehrels, W.R., Laborel, J., Wright, A.J., 2010. Paleoenvironmental records, geophysical modeling, and reconstruction of sea-level trends and variability on centennial and longer timescales. In: Church, J.A., Woodworth, P.L., Aarup, T., Wilson, W.S. (Eds.), *Understanding Sea-Level Rise and Variability*. Wiley-Blackwell, pp. 61–121.
- Lamb, H.H., 1965. The early medieval warm epoch and its sequel. *Palaeogeography, Palaeoclimatology, Palaeoecology* 1, 13–37.
- Lawler, A., 2011. Did the first cities grow from marshes? *Science* 331, 141.
- Makwana, N., Prizomwala, S.P., Chauhan, G., Phartiyal, B., Thakkar, M.G., 2019. Late Holocene palaeo-environmental change in the Banni Plains, Kachchh, Western India. *Quaternary International* 507, 197–205.
- Mandal, P., Rastogi, B.K., Satyanarayana, H.V.S., Kousalya, M., 2004. Results from local earthquake velocity tomography: implications toward the source process involved in generating the 2001 Bhuj earthquake in the lower crust beneath Kachchh (India). *Bulletin of the Seismological Society of America* 94, 633–649.
- Mann, T., Bender, M., Lorscheid, T., Stocchi, P., Vacchi, M., Switzer, A.D., Rovere, A., 2019. Holocene sea levels in southeast Asia, Maldives, India and Sri Lanka: the SEAMIS database. *Quaternary Science Reviews* 219, 112–125.
- Maurya, D.M., Thakkar, M.G., Chamyal, L.S., 2003. Quaternary geology of the arid zone of Kachchh: Terra incognita. *Proceedings of the Indian National Science Academy* 69, 125–135.
- McCarthy, T.S., Metcalfe, J., 1990. Chemical sedimentation in Okavango Delta, Botswana. *Chemical Geology* 89, 157–178.
- McLennan, S.M., 1993. Weathering and global denudation. *Journal of Geology* 101, 295–303.
- Merh, S.S., 2005. The great Rann of Kachchh: perceptions of a field geologist. *Journal of the Geological Society of India* 65, 9–25.
- Miall, A.D., 1977. Lithofacies types and vertical profile models in braided river deposits: a summary. *Geological Survey of Canada* 3303, 597–604.
- Michael, L., Gopala Rao, D., Krishna, K.S., Vora, K.H., 2009. Late Quaternary Seismic Sequence Stratigraphy of the Gulf of Kachchh, Northwest of India. *Journal of Coastal Research* 25, 459–468.
- Milliman, J.D., Quraishie, G.S., Beg, M.A.A., 1984. Sediment discharge from the Indus River to the ocean: past, present and future. In: Haq, B.U., Milliman, J.D. (Eds), *Marine Geology and Oceanography of Arabian Sea and Coastal Pakistan*. Van Nostrand Reinhold, New York, pp. 66–70.
- Milne, G.A., Long, A.J., Bassett, S.E., 2005. Modelling Holocene relative sea-level observations from the Caribbean and South America. *Quaternary Science Reviews* 24, 1183–1202.
- Mitrovica, J.X., Milne, G.A., 2002. On the origin of late Holocene sea-level high stands within equatorial ocean basins. *Quaternary Science Review* 21, 2179–2190.
- Mitrovica, J.X., Peltier, W.R., 1991. On postglacial geoid subsidence over the equatorial oceans. *Journal of Geophysical Research: Solid Earth*, 96(B12), 20053–20071.
- Murray, A.S., Wintle, A.G., 2000. Luminescence dating of quartz using an improved single-aliquot regenerative-dose protocol. *Radiation Measurements* 32, 57–73.
- Nanson, G.C., Tooth, S., 1999. Arid-zone rivers as indicators of climate change. In Singhvi, A.K. and Derbyshire, E., (eds), *Paleoenvironmental reconstruction in arid lands*, Rotterdam: A.A. Balkema, 175–216.
- Nayar, T.S., 1990. *Pollen flora of Maharashtra State, India*. Today and Tomorrow's Printers and Publishers, New Delhi, pp. 1–139.
- Nazneen, S., Raju, N.J., 2017. Distribution and sources of carbon, nitrogen, phosphorous and biogenic silica in the sediments of Chilika lagoon. *Journal of Earth System Science* 126, 1–13.
- Newman, W.S., Pardi, R.W., Fairbridge, R.W., 1989. Some considerations of the compilation of late Quaternary sea level curves: A North American perspective. In: Scott D.B., Pirazzoli P.A., Honig C.A. (eds) *Late Quaternary Sea-Level Correlation and Applications*. NATO ASI Series (Series C: Mathematical and Physical Sciences) 256. Springer, Dordrecht. https://doi.org/10.1007/978-94-009-0873-4_11
- Ngangom, M., Bhandari, S., Thakkar, M.G., Shukla, A.D., Juyal, N., 2016. Mid-Holocene extreme hydrological events in the eastern Great Rann of Kachchh, western India. *Quaternary International* 443, 188–199.
- Orton, G.J., Reading, H.G., 1993. Variability of deltaic processes in terms of sediment supply, with particular emphasis on grain-size. *Sedimentology* 40, 475–512.
- Otvos, E.G., 2000. Beach ridges—definitions and significance. *Geomorphology* 32, 83–108.
- Pant, R.K., Juyal, N., 1993. Late Quaternary coastal instability and sea level changes: new evidence from Saurashtra coast, Western India. *Zeitschrift für Geomorphologie N.F.* 37, 29–40.
- Patel, S.J., Desai, B.G., 2009. Animal-sediment relationship of the crustaceans and polychaetes in the intertidal zone around Mandvi, Gulf of Kachchh, Western India. *Journal of the Geological Society of India* 74, 233–259.
- Peltier, W.R., 1999. Global sea level rise and glacial isostatic adjustment. *Global Planetary Change* 20, 93–123.
- Pirazzoli, P.A., 1991. *World Atlas of Holocene sea-level changes*. Elsevier, Amsterdam.
- Prahl, F.G., Bennett, J.T., Carpenter, R., 1980. The early diagenesis of aliphatic hydrocarbons and organic matter in sedimentary particulates from Dabob Bay, Washington. *Geochimica et Cosmochimica Acta* 44, 1967–1976.
- Prizomwala, S.P., Das, A., Chauhan, G., Solanki, T., Basavaiah, N., Bhatt, N., Thakkar, M.G., Rastogi, B.K., 2016. Late Pleistocene–Holocene uplift driven terrace formation and climate-tectonic interplay from a seismically active intraplate setting: An example from Kachchh, western India. *Journal of Asian Earth Sciences* 124, 55–67.
- Rajendran, C.P., Rajendran, K., 2002. Historical constraints on previous seismic activity and morphologic changes near the source

- zone of the 1819 Ran of Kachchh earthquake: further light on the penultimate event. *Seismological Research Letters* 73, 470–479.
- Ramaswamy, V., Nath, B.N., Vethamony, P., Illangovan, D., 2007. Source and dispersal of suspended sediment in the macro-tidal Gulf of Kachchh. *Marine Pollution Bulletin* 54, 708–719.
- Rao, S.R., 2000. Lothal: a Harappan port town. In: Lahiri, N. (Ed.), *Decline and Fall of the Indus Civilization*. Permanent Black, Delhi, pp. 146–15.
- Rao, V.P., Rajagopalan, G., Vora, K.H., Almeida, F., 2003. Late Quaternary sea level and environmental changes from relic carbonate deposits of the western margin of India. *Proceedings of the Indian Academy of Science (Earth Planetary Science)* 112, 1–25.
- Rawat, Y.S., 2015. Coastal Sites; Possible Port Towns of Harappan time in Gujarat. In: Keller, S., Pearson, M. (Eds.), *Port Towns of Gujarat*. Primus Books, pp. 187–215.
- Ray, D., Shukla, A.D., 2018. The Mukundpura meteorite, a new fall of CM chondrite. *Planetary & Space Science* 151, 149–154.
- Reid, I., Frostick, L.E., 1997. Channel form, flows and sediments in deserts. In: Thomas, D.S.G. (Ed.), *Arid Zone Geomorphology*. 2nd ed. John Wiley & Sons, pp. 205–229.
- Reimer, P.J., Bard, E., Bayliss, A., Beck, J.W., Blackwell, P.G., Ramsey, C.B., Buck, C.E., et al., 2013. IntCal13 and Marine13 radiocarbon age calibration curves 0–50,000 years cal BP. *Radiocarbon* 55, 1869–1887.
- Rick, J.Y., James, T.L., Daidu, F., George, S.B., Hui-Ling, L., Ting-Ting, C., 2017. Land-sea duel in the late Quaternary at the mouth of a small river with high sediment yield. *Journal of Asian Earth Science* 143, 59–76.
- Rovere, A., Raymo, M.E., Vacchi, M., Lorscheid, T., Stocchi, P., Gomez-Pujol, L., Harris, D.L., Casella, E., O’Leary, M.J., Hearty, P.J., 2016. The analysis of Last Interglacial (MIS 5e) relative sea-level indicators: Reconstructing sea-level in a warmer world. *Earth-Science Reviews* 159, 404–427.
- Roy, B., Merh, S.S., 1982. The Great Rann of Kutch: an intriguing Quaternary terrain. *Recent Research in Geology* 29, 519–539.
- Sampei, Y., Matsumoto, E., Kamei, T., Tokuoka, T., 1997. Sulfur and organic carbon relationship in sediments from coastal brackish lakes in the Shimane peninsula district, southwest Japan. *Geochemical Journal* 31, 245–262.
- Sarkar, A., Deshpande-Mukherjee, A., Bera, M.K., Das, B., Juyal, N., Morthekai, P., Deshpande, R.D., Shinde, V.S., Rao, L.S., 2016. Oxygen isotope in archaeological bioapatites from India: Implications to climate change and decline of Bronze age Harappan civilization. doi: 10.1038/srep26555.
- Sarkar, A., Mukherjee, A.D., Sharma, S., Sengupta, T., Ram, F., Bera, M.K., Bera, S., et al., 2020. New evidence of early Iron Age to Medieval settlements from the southern fringe of Thar Desert (western Great Rann of Kachchh), India: Implications to climate-culture co-evolution. *Archaeological Research in Asia* 21, p.100163.
- Schulz, H., von Rad, U., Erlenkeuser, H., 1998. Correlation between Arabian Sea and Greenland climate oscillations of the past 110,000 years. *Nature* 393(6680), 54–57.
- Semeniuk V., 2005. Tidal Flats. In: Schwartz, M.L. (Ed.), *Encyclopedia of Coastal Science*. Springer, Dordrecht. https://doi.org/10.1007/1-4020-3880-1_317
- Sengupta, T., Deshpande Mukherjee, A., Bhushan, R., Ram, F., Bera, M.K., Raj, H., Dabhi, A.J., et al., 2020. Did the Harappan settlement of Dholavira (India) collapse during the onset of Meghalayan stage drought? *Journal of Quaternary Science* 35, 382–395.
- Sharma, S., Chand, P., Bisht, P., Shukla, A.D., Bartarya, S.K., Sundriyal, Y.P., Juyal, N., 2016. Factors responsible for driving the glaciation in the Sarchu plain, eastern Zaskar Himalaya, during the late quaternary. *Journal of Quaternary Science* 31, 495–51.
- Sharma, S., Shukla, A.D., 2018. Factors governing the pattern of glacier advances since the Last Glacial Maxima in the transitional climate zone of the Southern Zaskar Ranges, NW Himalaya. *Quaternary Science Reviews* 201, 223–240.
- Shennan, I., 2015. Handbook of sea-level research: Framing Research Questions. In: Shennan, I., Long, A.J., Horton, B.P. (Eds.), *Handbook of sea-level research*. John Wiley & Sons, West Sussex, UK, pp. 536–553.
- Shennan, I., Horton, B., 2002. Holocene land and sea-level changes in Great Britain. *Journal of Quaternary Science* 17, 511–526.
- Shennan, I., Long, A.J., Horton, B.P. (Eds.), 2015. *Handbook of sea-level research*. John Wiley & Sons, West Sussex, UK.
- Shukla, A.D., Bhandari, N., Shukla, P.N., 2002. Chemical signatures of the Permian-Triassic transitional environment in Spiti valley, India proceedings of catastrophic events and mass extinction: impacts and beyond. *Geological Society of America Special Papers* 356, 445–454
- Snelgrove, R., 1979. Migration of the Indus river, Pakistan in response to plate tectonic motion. *Journal of the Geological Society of India* 20, 392–403.
- Srivastava, K.M., 1991. *Madinat Hamad Burial Mounds—1984–85*. Bahrain National Museum.
- Stanley, D.J., Warne, A.G., 1997. Holocene sea level changes and early human utilization of deltas. *GSA Today* 7, 1–7.
- Stein, A., 1931. *An archaeological tour in Gedrosia*. <http://csreposito.nvli.in/handle/123456789/8617>.
- Stuiver, M., Reimer, P.J., 1993. Extended 14C Data Base and Revised CALIB 3.0 14C Age Calibration Program. *Radiocarbon* 35, 215–230.
- Tankard, A.J., Rogers, J., 1978. Late Cenozoic palaeoenvironments on the west coast of southern Africa. *Journal of Biogeography* 5, 319–337.
- Taylor, M., Stone, G.W., 1996. Beach-Ridges: A Review. *Journal of Coastal Research* 12, 612–621.
- Taylor, S.R., McLennan, S.M., 1985. *The continental crust: its composition and evolution*. Blackwell Scientific Publication, Carlot.
- Thanikaimoni, G., 1987. *Mangrove Palynology*. UNDP/UNESCO Regional Project on Training and Research on Mangrove Ecosystems, RAS/79/002, and the French Institute, Pondicherry.
- Therrien, F., 2006. Depositional environments and fluvial system changes in the dinosaur bearing Sanpetru Formation (Late Cretaceous, Romania): post-orogenic sedimentation in an active extensional basin. *Sedimentary Geology* 192, 183–205
- Thomas, P.J., Juyal, N., Kale, V.S., Singhvi, A.K., 2007. Luminescence chronology of late Holocene extreme hydrological events in the upper Penner river basin, South India. *Journal of Quaternary Science* 22, 747–753.
- Tooth, S., 2000. Process, form and change in dry land rivers: a review of recent research. *Earth-Science Reviews* 51, 67–107
- Tyagi, A.K., Shukla, A.D., Bhushan, R., Thakker, P.S., Thakkar, M.G., Juyal, N., 2012. Mid-Holocene sedimentation and landscape evolution in the western Great Rann of Kachchh, India. *Geomorphology* 151, 89–98.
- Unnikrishnan, A.S., Gouveia, A.D., Vethamony, P., 1999. Tidal regime in Gulf of Kutch, west coast of India, by 2D model. *Journal of waterway, port, coastal, and ocean engineering* 125, 276–284.

- Vacchi, M., Engelhart, S.E., Nikitina, D., Ashe, E.L., Peltier, W.R., Roy, K., Kopp, R.E., Horton, B.P., 2018. Postglacial relative sea-level histories along the eastern Canadian coastline. *Quaternary Science Reviews* 201, 124–146.
- Vacchi, M., Rovere, A., Chatzipetros, A., Zouros, N., Firpo, M., 2014. An updated database of Holocene relative sea level changes in NE Aegean Sea. *Quaternary International* 328, 301–310.
- van de Plassche, O., van der Borg, K., de Jong, A.F., 1998. Sea level–climate correlation during the past 1400 yr. *Geology* 26, 319–322.
- Vethamony, P., Babu, M.T., 2010. Physical processes in the Gulf of Kachchh: A review. volumes from the Last Glacial Maximum to the Holocene. *Proceedings of the National Academy of Science* 111, 497–503.
- Vora, K.H., Wagle, B.G., Veerayya, M., Almeida, F., Karisiddaiah, S.M., 1996. 1300 km long late Pleistocene–Holocene shelf edge barrier reef system along the western continental shelf of India: occurrence and significance. *Marine Geology* 134, 145–162.
- Wang, P., 2012. Principles of sediment transport applicable in tidal environments. In: Davis Jr., Richard A., Dalrymple, Robert W. (Eds.) *Principles of Tidal Sedimentology*. Springer, Dordrecht, pp. 19–34.
- Wegmann, K.W., Pazzaglia, F.J., 2009. Late Quaternary fluvial terraces of the Romagna and Marche Apennines, Italy: Climatic, lithologic, and tectonic controls on terrace genesis in an active orogen. *Quaternary Science Reviews* 28, 137–165.
- Wells, J.T., Coleman, J.M., 1984. Deltaic morphology and sedimentology, with special reference to the Indus River delta. In: Haq, B.U., Milliman, J.D. (Eds.), *Marine Geology and Oceanography of Arabian Sea and Coastal Pakistan*, Louisiana State University, LA.
- Whitehouse, P.L., 2018. Glacial isostatic adjustment modelling: historical perspectives, recent advances, and future directions. *Earth Surface Dynamics* 6, 401–429.
- Willis, B.J., Behrensmeier, A.K., 1994. Architecture of Miocene over bank deposits in northern Pakistan. *Journal of Sedimentary Research* B64, 60–67.
- Woodroffe, C.D., McLean, R.F., Polach, H., Wallensky, E., 1990. Sea level and coral atolls: Late Holocene emergence in the Indian Ocean. *Geology* 18, 62–66.
- Wright, R.P., Bryson, R.A., Schuldenrein, J., 2008. Water supply and history: Harappa and the Beas regional survey. *Antiquity* 82, 37–48.
- Yadava, M.G., Ramesh, R., 1999. Speleothems—useful proxies for past monsoon rainfall. *Journal of Scientific and Industrial Research* 58, 339–348.